ABSTRACT

Title of document: INVESTIGATION OF NOVEL MEMBRANE TECHNOLOGIES FOR HYDROGEN SEPARATION

William M. Van Cleave, Master of Science, 2017

Thesis directed by: Professor Ashwani K. Gupta
Department of Mechanical Engineering

The production of hydrogen gas via its separation from multicomponent syngas derived from biomass is an important process in the burgeoning carbon-neutral hydrogen economy. Current methods utilize membranes made from expensive materials such as palladium or bulky pressure vessels that use adsorption properties. Holey graphene and doped perovskite ceramics are alternative membrane materials that are relatively inexpensive and easily produced. A range of holey graphene membranes was produced using dry pressing and other techniques, including high temperature reduction, to examine the efficiency of this material. Experimental results using these holey graphene membranes are presented from a lab-scale facility designed to test various membrane types. These results showed decreasing flux and increasing selectivity as membrane thickness increased. Comparison with results from literature indicate these membranes exhibit higher overall flux but lower selectivity when compared to palladium-based membrane technologies.

INVESTIGATION OF NOVEL MEMBRANE TECHNOLOGIES FOR HYDROGEN SEPARATION

by

William M. Van Cleave III

Thesis submitted to the Faculty of the Graduate School of the
University of Maryland, College Park in partial fulfillment
of the requirements for the degree of
Master of Science
2017

Advisory Committee:
Professor Ashwani K. Gupta, Chair/Advisor
Dr. Eric Wachsman, Professor
Dr. Bao Yang, Professor

Dedication

To Lauren.

Acknowledgments

I owe an enormous debt of gratitude to all those who have helped me turn this thesis into a reality and who have supported me during my graduate experience.

I'd like to thank my advisor, Professor Ashwani Gupta for providing me with the opportunity to work on challenging and interesting research over the past two years. His advice and guidance were invaluable and it has been a pleasure to work with and learn from such an extraordinary individual.

The members of the Combustion Laboratory provided me with assistance and advice on innumerable occasions and deserve a special mention. Dr. Ahmed Khalil, Ahmed ElMelih, Kiran Raj Burra, and Parth Kathrotiya helped me many times, both academically and in my research. Additionally, my research partners in the Department of Materials Science, Steve Lacey, Eugene Ostrovskiy, and Mann Sakbodin, each contributed expertise and time into the success of this project.

I would also like to thank the United States Coast Guard for providing me the opportunity to pursue my Master's Degree through the Naval Engineering Advanced Education Program. Additionally, CDR David Clippinger, CDR Jessica Rozzi-Ochs, LCDR Matthew Weber, LCDR Jan Rybka and LCDR Lucas Marino have each personally contributed to my personal and professional development.

None of this would have been possible without the support of my parents, Bill and Ann. Their support and encouragement has helped me immensely. Finally, I would like to especially thank my beautiful wife, Lauren. Her advice, motivation, patience and unwavering support has meant the world to me over the past two years.

Table of Contents

List of Tables

List of Figures

List of Abbreviations

$OH^{\cdot}_{O}$	Hydroxyl Ion (Kröger-Vink notation)
BBP	Benzyl Butyl Phthalate
BLG	Bi-Layer Graphene
CDRM	Carbon Dioxide Reforming of Methane
CMS	Carbon Molecular Sieving
CVD	Chemical Vapor Deposition
EPC	Electronic Pressure Control
FLG	Few-Layer Graphene
GC	Gas Chromatograph
GO	Graphene Oxide
hG	Holey Graphene
HPLC	High Pressure Liquid Chromatography
LHV	Low Heating Value
MHV	Medium Heating Value
NETL	National Energy Technology Laboratory
PSA	Pressure Swing Adsorption
PVB	Polyvinyl Butyral
PVD	Physical Vapor Deposition
rGO	Reduced Graphene Oxide
RSS	Root Sum of Squares
SEM	Scanning Electron Microscopy
TCD	Thermal Conductivity Detector
TEM	Transmission Electron Microscopy
TMD	Transition Metal Dichalcogenides
TMO	Transition Metal Oxide
WGS	Water-Gas Shift (Reaction)

Chapter 1: Motivation and Objectives

As the world continues to transition away from traditional hydrocarbon energy sources due to concerns about climate change, energy security, and pollution, hydrogen-based energy solutions present an attractive, high mass energy density (120.7 kJ/g), potentially zero-carbon option for energy generation [1]. Most current hydrogen gas production is via steam-based processing of either coal or natural gas due to their wide availability and low cost. An alternative production method uses biomass as the source material [2]. In each of these methods, the hydrogen gas must be separated out of a synthesis gas (syngas) mixture that also includes carbon dioxide, carbon monoxide, methane, and water vapor. Using biomass as the source material is particularly attractive because of its potential to be carbon-neutral [3].

This separation step is often performed using a variety of metal, ceramic, or polymer membranes, with varying degrees of efficiency and cost effectiveness [4]. Every membrane technology utilizes one of four separation mechanisms: Knudsen diffusion, molecular sieving, solution-diffusion, and surface diffusion [5]. Palladium and palladium-based alloy membranes in particular have received significant research interest in the recent past due to their ability to produce high-purity permeate gas [6–9]. However, these membranes are limited by required operating temperatures of 300 °C to 600 °C and their high cost [10].

A novel alternative membrane technology is the use of so-called holey graphene as a membrane material. This material is formed by partially oxidizing graphene in order to introduce nano-scale pores that result in a selectively porous material [11]. These holey graphene membranes operate via a molecular sieving mechanism and do not experience the hydrogen embrittlement prevalent in dense palladium membranes. They are also significantly less costly to produce than traditional dense membranes [11]. This study examines the selective diffusion of hydrogen through these holey graphene membranes and investigates the effects of membrane thickness and density, as well as the effects of high-temperature partial reduction of the membrane material. Examination of the behavior of these membranes promotes the creation of further solutions to obtain high-purity hydrogen gas for use in the emerging hydrogen economy.

Chapter 2: Literature Review

2.1 Overview

The separation of hydrogen from a multiple-component gas has been an area of significant research since the discovery of hydrogen as a potential fuel source [12]. Because large quantities of naturally occurring pure hydrogen gas are not found outside of stars, production and purification efforts have necessarily been pursued alongside research into the use of hydrogen as a fuel source itself. Hydrogen separation methods fall into one of three categories: physical (via pressure swing adsorption, cryogenic distillation, or metal hydride separation), chemical (with catalytic purification), and selective diffusion (using various membranes) [13]. Selective diffusion is the oldest purification technique, dating back to the middle of the 19th century. Though it has largely been supplanted by pressure swing adsorption for industrial-scale hydrogen purification, selective diffusion is still a pivotal hydrogen separation technology widely used for small- and medium-scale purification operations [5].

2.2 Gasification and Syngas Creation

Large-scale hydrogen gas production necessarily involves the production of a gas mixture from which pure hydrogen is then extracted. For research purposes this gas mixture is generally created by combining specific ratios of pure gases, but in industry this mixture, referred to as syngas, is most often the product of a process called gasification. Through gasification, low-grade fuels such as biomass, plastics, or any other carbonaceous fuel can be converted into usable gaseous fuels [14]. Syngas is one key to the creation of a hydrogen economy and reducing the world's reliance on fossil fuels.

2.2.1 Syngas Production

Gasification is the process of heating a solid, liquid, or gaseous carbonaceous material with a gasifying agent in order to produce gaseous products with useful residual heating values. This process is distinct from combustion, which produces gases without any useful heating value. Partial oxidation, pyrolysis and hydrogenation are all included in the umbrella of gasification technologies, however. Generally speaking, during the gasification process, the organic matter is first pyrolized by heating it in the absence of oxygen. This produces char, tars, and LHV to MHV fuel gas. These products are then gasified, breaking down the methane present in the fuel gas to produce syngas and ash [14, 15]. The specific gasifying agent used during gasification is chosen based on the desired syngas composition. For hydrogen production, steam is an effective gasifying agent. The gasification process is also highly dependent on the source material, the temperature and pressure at which the reaction occurs, and the ratio of steam to carbon [16].

The gasification process of solid carbon is governed by several equations, including the combustion reactions:

$$\mathrm{C} + \frac{1}{2}\,\mathrm{O_2} \longrightarrow \mathrm{CO} \qquad -111\,\mathrm{MJ/kmol}, \tag{2.1}$$

$$\mathrm{CO} + \frac{1}{2}\,\mathrm{O_2} \longrightarrow \mathrm{CO_2} \qquad -283\,\mathrm{MJ/kmol}, \tag{2.2}$$

$$\mathrm{H_2} + \frac{1}{2}\,\mathrm{O_2} \longrightarrow \mathrm{H_2O} \qquad -242\,\mathrm{MJ/kmol}, \tag{2.3}$$

the Boudouard reaction:

$$\mathrm{C} + \mathrm{CO_2} \rightleftharpoons 2\,\mathrm{CO} \qquad +172\,\mathrm{MJ/kmol}, \tag{2.4}$$

the water gas reaction:

$$\mathrm{C} + \mathrm{H_2O} \rightleftharpoons \mathrm{CO} + \mathrm{H_2} \qquad +131\,\mathrm{MJ/kmol}, \tag{2.5}$$

and the methanation reaction:

$$\mathrm{C} + 2\,\mathrm{H_2} \rightleftharpoons \mathrm{CH_4} \qquad -75\,\mathrm{MJ/kmol}. \tag{2.6}$$

Because combustion should not occur during gasification, the process is by and large governed by equations 2.4, 2.5, and 2.6. These equations can be reduced to the following two-equation

system in situations where there is complete or near-complete carbon conversion [14]:

$$\mathrm{CO} + \mathrm{H_2O} \rightleftharpoons \mathrm{CO_2} + \mathrm{H_2} \qquad -41\,\mathrm{MJ/kmol}, \tag{2.7}$$

$$\mathrm{CH_4} + \mathrm{H_2O} \rightleftharpoons \mathrm{CO_2} + 3\,\mathrm{H_2} \qquad +206\,\mathrm{MJ/kmol}. \tag{2.8}$$

Equation 2.7 is referred to as the water-gas shift (WGS) reaction, and equation 2.8 is referred to as the steam methane reforming reaction. A simplified diagram of the gasification reaction sequence for coal or biomass is shown in figure 2.1.

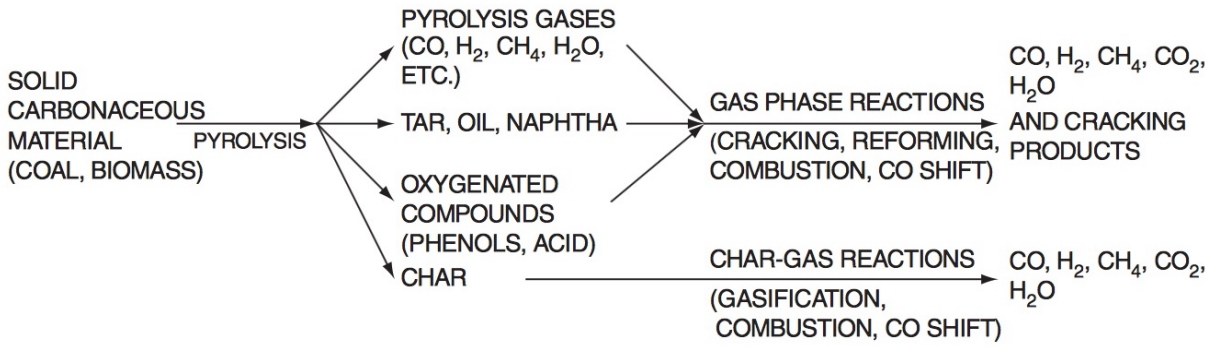

Figure 2.1: Simplified reaction sequence for pyrolysis and gasification of coal or biomass [14].

2.2.2 Syngas Composition and Use

The gasification of biomass (often cellulose- or animal waste-based) results in a syngas composed largely of hydrogen, carbon monoxide, and carbon dioxide, along with small amounts of water vapor, methane, and heavier hydrocarbons [14, 17, 18]. Table 2.1 lists syngas compositions obtained using various source materials. In many cases, the water vapor present in the product gas is condensed out shortly after production in order to remove tars from the mixture [19]. Additionally, trace amounts of a variety of impurities are also often

Table 2.1: Composition of oil-derived and biomass-derived syngas observed in several studies. All values are in mol%.

Source Material	H_2	CO	CO_2	H_2O	CH_4	Other
Oil in O_2 and steam (Higman et al.) [14]	34.0%	63.2%	0.1%	0.2%	0.3%	2.2%
Hemicellulose in N_2 (Yang et al.) [17]	33.8%	20.8%	37.6%	–	6.1%	1.6%
Cellulose in N_2 (Yang et al.) [17]	22.8%	41.2%	27.3%	–	7.6%	1.0%
Lignin in N_2 (Yang et al.) [17]	50.2%	20.4%	18.8%	–	9.6%	1.1%
Cellulose in N_2 (Asadullah et al.) [3]	16.3%	54.7%	16.3%	–	12.7%	–
Chicken Litter in air (Joseph et al.) [18]	17.5%	21.0%	31.3%	25.6%	3.8%	0.8%

present, including sulfur, nitrogen, and argon [14]. This mixture can be used in a variety of processes, including direct combustion, or it can be separated into its constituent parts for use as pure gases. In many cases, it is economically and environmentally advantageous to separate hydrogen from the remaining gases. By doing so, it is possible to use the pure hydrogen gas in fuel cells or other industrial applications. This need is what drove research into hydrogen separation technologies [20–22].

2.3 Hydrogen Separation

2.3.1 History of Hydrogen Separation Research

The discovery by Henri Sainte-Claire Deville and Louis Troost of hydrogen diffusion through heated homogenous platinum and iron plates in 1863 is the first known instance of hydrogen gas diffusion through a metal membrane [23, 24]. Thomas Graham continued

investigations of hydrogen permeation through films and tubes and discovered that palladium is particularly efficient at absorbing hydrogen, especially at elevated temperatures [25]. This is due in particular to palladium's unique lattice structure, which supports high catalytic activity and hydrogen selectivity [26]. Work continued on palladium membrane separation methods for the next several decades without significant advancements, due largely to excessive distortion caused by a partial $\alpha \rightarrow \beta$ phase change at temperatures below 300 °C and pressures below 20 atm (roughly 2 MPa) [27]. Local stresses could be minimized by operating the membrane in conditions that forced a complete phase change (shown in Figure 2.2), but this required extensive purging periods and still subjected the membrane to uniform expansion and contraction during the phase change [28].

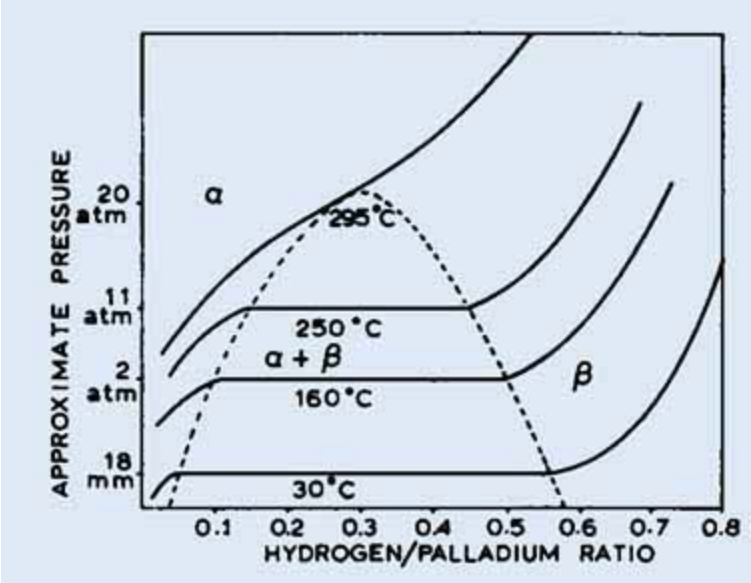

Figure 2.2: Pure Palladium undergoes an $\alpha \rightarrow \beta$ phase change when exposed to hydrogen at low temperatures, leading to significant distortion [28].

Practical applications of these results would have to wait until 1956, when James Hunter, working for The Atlantic Refining Company, patented a silver-palladium film containing between 10% and 50% silver for use in hydrogen separation. Alloying palladium

with silver in this way both increased the hydrogen diffusion rate and suppressed the phase change-induced lattice expansion experienced by pure palladium membranes, as shown in figure 2.3 [29]. This discovery opened the door to full commercialization of hydrogen separation in the early 1960s using an alloy comprised of 77% palladium and 23% silver [30].

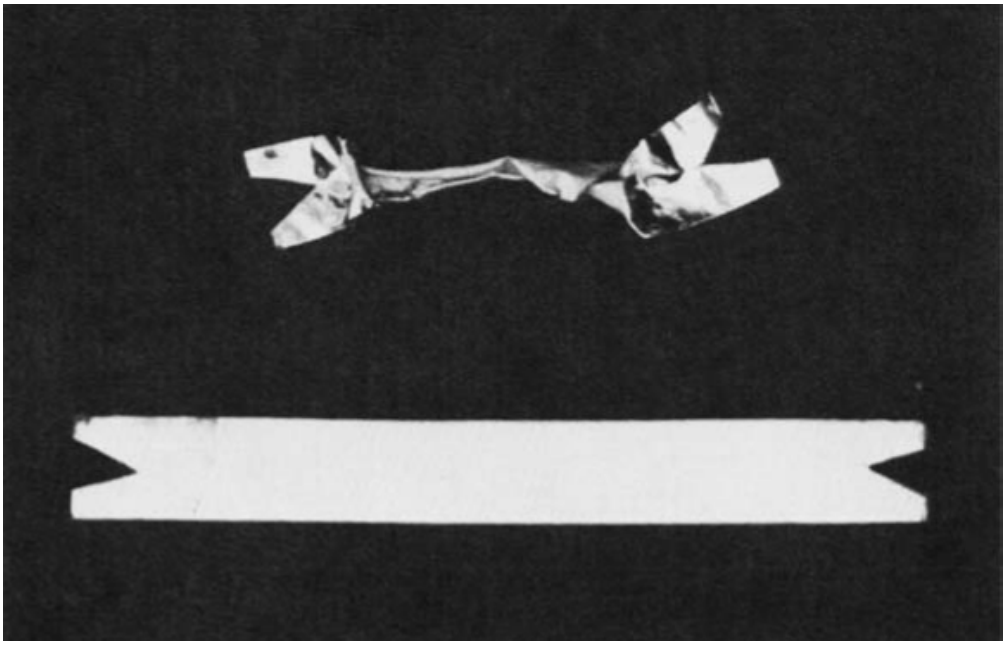

Figure 2.3: Material samples exposed to repeated heating and cooling in hydrogen atmospheres. Pure palladium is on the top; palladium-silver alloy on the bottom. Distortion of the pure palladium sample is due to the phase change described in figure 2.2 [13].

Some alternative membrane types began to receive attention in the early 2000s: micro-porous ceramic-based membranes [31–33], dense ceramic-based membranes [34–40] and so-called carbon molecular sieving (CMS) membranes [41–43]. These membranes attempt to address several of the issues with palladium-based membranes, including high cost, susceptibility to hydrogen embrittlement, and sensitivity to feed gas contaminants such as hydrogen sulfide [5].

While the commercialization of palladium membrane-based hydrogen separation technologies was still in progress, physical separation methods (i.e., cryogenic distillation

and pressure swing adsorption) were introduced. These methods have gained popularity in large-scale hydrogen production schemes due to scalability [13]. Pressure swing adsorption (PSA) was introduced in the late 1970s and utilizes repeated pressure changes in vessels containing specially designed adsorbents to extract one less-readily adsorbed product (in this case hydrogen) from a feed stream made up of multiple components, as shown in Figure 2.4 [44].

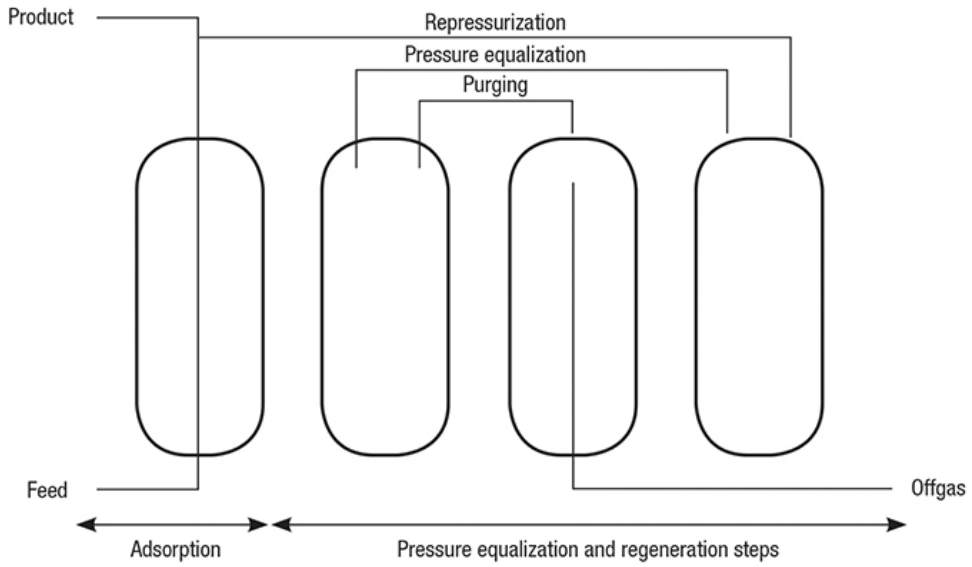

Figure 2.4: Simplified pressure swing adsorption system diagram [45].

Although this method has the potential to provide a large volume of high-purity product, there are several disadvantages. Because it is fundamentally a batch process, PSA requires multiple pressure vessels designed to withstand very high pressures in order to produce a relatively constant product stream [46]. Additionally, it is not possible to extract all of the desired product from the feed stream, although the recovered portion can be increased via more complex flow paths [44]. The cryogenic distillation method was developed around the same time and relies on differences in the condensation temperatures

of gases to separate components out of a mixed feed stream. Like pressure swing adsorption, this process is best suited for large, industrial-scale concerns. It also allows for recovery of a larger portion of the desired product gas, but at decreased purity levels [13]. Though both of these methods have advantages that suit them to large-scale industrial hydrogen production, comparatively enormous capital costs and limitations with either the recovery percentage or product purity prevent them from being a hydrogen manufacturing panacea.

2.3.2 Current Separation Research

Current state-of-the-art hydrogen separation research centers around improvements to the PSA process as well as the identification of alternative metal or ceramic membrane technologies. Researchers have investigated modifications to the PSA process to allow for the extraction of hydrogen from feed gas streams with non-standard impurity proportions [47] and the impacts of temperature on the breakthrough curves of various adsorbents [48]. Research has also been done into the effectiveness of supplementing a PSA process with membranes placed either upstream or downstream of the PSA unit [49]. This and other research being done in this field show the potential for modest improvements to hydrogen yield and purity via the PSA process, but no disruptive breakthroughs.

Similarly, current membrane separation research is focused on exploring various materials and manufacturing processes for their suitability as alternatives to traditional palladium-silver membranes due to high cost, continued hydrogen embrittlement concerns, and the potential for feed gas components (especially sulphur and carbon compounds) to damage the membrane [50]. Research is ongoing in the use of several alternative metal

membranes: pure vanadium, niobium, and tantalum have hydrogen permeabilities much higher than palladium and are cheaper; binary alloys of palladium with copper, yttrium, gold, cesium, and nickel have the potential for increased thermal and chemical stability; and multi-component alloys of palladium using up to five additional metals to take advantage of the benefits of each [5]. Thin-film membrane construction techniques are also being explored, to include sputtering, electrodeposition, electroless plating, chemical and physical vapor deposition (CVD/PVD), and spray pyrolysis [4]. These techniques allow for the creation of structurally sound membranes with less palladium (and alloying metal) content by depositing a thin layer of the membrane metal on a porous substrate [5]. All of this research is a direct response to the disadvantages posed by existing palladium and palladium alloy membranes, and takes the form of incremental improvements rather than transformative breakthroughs.

2.4 Permeation Mechanisms and Modeling

In contrast to hydrogen separation methods using physical or chemical processes, membraneous separation technologies employ a barrier across the flow path that only allows hydrogen to pass through, while excluding all other molecule types. In membrane gas separation operations, the gas that is input into a system for separation is called the feed gas. Gas that passes through the membrane is called the permeate, while gas that is excluded by the membrane is called the retenate. In some cases, an additional gas, referred to as the sweep gas, is used on the downstream side of the membrane to transport permeate away from the membrane. In a similar vein, the faces of the membrane itself are called the upstream

(feed) side and the downstream (sweep) side. Generally speaking, these barriers operate via one of five mechanisms: Knudsen diffusion, molecular sieving, surface diffusion, capillary condensation, and solution-diffusion [8]. While different, these mechanisms all permit some molecular species to pass through otherwise impermeable materials. Figure 2.5 depicts how these mechanisms work, along with a diagram of uninterrupted flow through a pore too large to induce separation (Pouselle flow). Of particular interest in hydrogen separation are solution-diffusion and molecular sieving.

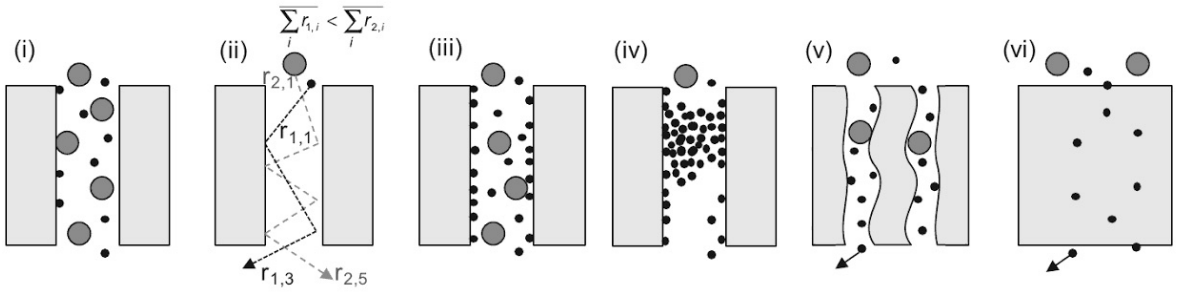

Figure 2.5: Depictions of different diffusion mechanisms: (i) Pouselle flow (no diffusion), (ii) Knudsen diffusion, (iii) Molecular sieving, (iv) Surface diffusion, (v) Capillary condensation, (vi) Solution-diffusion [8].

2.4.1 Mechanism Operating Principles

Knudsen diffusion relies on differences between the mean free paths of different molecular species: Molecules with smaller mean free paths are more likely to diffuse through the membrane material than those with larger mean free paths. Molecular sieving is instead due to differences in the kinetic diameters of molecules, which allows for diffusion through even smaller pores than Knudsen diffusion, and is the mechanism most similar to conventional sieving; e.g., a baseball cannot fit through a hole sized for a golf ball. In surface diffusion, one species of molecule adsorbs onto the pore wall surface and travels along it to

the other side of the membrane. Species that are not adsorbable cannot transit through the pore. This is often seen in combination with Knudsen diffusion. In capillary condensation, the membrane's pores are filled with the condensed form of the desired permeate, which allows only this molecular species to pass through. In solution-diffusion, the transport of the permeate across the membrane proceeds in five steps [8]:

1. Adsorption of the molecule onto the membrane surface.

2. Dissolution of the molecule into ions, atoms, or other, smaller molecules.

3. Transport through the body of the membrane.

4. Reassociation of the ions, atoms or component molecules into the original molecule.

5. Desorption off of the downstream membrane surface.

Solution-diffusion is the mechanism by which the vast majority of hydrogen separation membranes, those composed of non-porous palladium and palladium alloys, operate. Because of their non-porous nature, these membranes have the ability to produce extremely high-purity permeate gas (up to 99.9999%) when compared to membranes using other diffusion mechanisms [13]. Dense ceramic membranes also utilize solution-diffusion and therefore have similarly high hydrogen selectivity [5]. By comparison, the holey graphene membranes used in this study, along with micro-porous ceramic and CMS membranes, operate via molecular sieving, with CMS membranes also experiencing some surface diffusion [8]. Although these types of membranes exhibit significant scalability and commercialization advantages (cost, chemical resistance, durability), the major tradeoff is a

significantly lower range of hydrogen selectivity, with selectivity ratios ranging from 4:1 to 139:1 [5].

2.4.2 Modeling Considerations

Diffusion of a fluid, referred to as the permeate, from the upstream (or feed) side to the downstream (or sweep) side of a membrane is described, at a high level, by two parameters: flux and selectivity. The flux, or amount of permeate transfer through the membrane, has units of mol/(min m^2) and is modeled by Fick's first law [26, 51, 52]:

$$J_{\mathrm{H}} = -D_M \frac{\partial C_{\mathrm{H}}}{\partial x}, \tag{2.9}$$

where J_{H} is the diffusion flux of hydrogen in the membrane, D_M is the diffusion coefficient of the membrane, and $\frac{\partial C_{\mathrm{H}}}{\partial x}$ is the change in hydrogen concentration across the membrane. In the case of steady-state flow through a non-porous membrane, the equilibrium hydrogen concentration within the membrane's structure $C_{\mathrm{H},eq}$ can be related to the partial pressure of hydrogen p_{H_2} through Sieverts' law:

$$C_{\mathrm{H},eq} = K_S \left(p_{\mathrm{H}_2}\right)^{1/2}, \tag{2.10}$$

where K_S is Sieverts' constant, p_{H_2} is the partial pressure of hydrogen, and the $\frac{1}{2}$ exponent indicates the dissociation of hydrogen molecules into two individual hydrogen atoms on the surface of the membrane, although it is important to note that a value of $\frac{1}{2} < n < 1$ is sometimes used to empirically tune the model [26, 51]. In order to help transform this

equation into a more useable form, we define the hydrogen activity a_{H}, which modifies the hydrogen concentration value within the membrane structure to account for deviations from idealized behavior, as

$$a_{\mathrm{H}} = \left(\frac{p_{\mathrm{H}_2}}{p^{\circ}_{\mathrm{H}_2}} \right)^{1/2}. \tag{2.11}$$

Note that the exponent is identical to that in equation 2.10, which, assuming local equilibrium, allows us to rearrange equation 2.11 and substitute it into equation 2.9, producing the following:

$$J_{\mathrm{H}} = -D_M K_S \left(p^{\circ}_{\mathrm{H}_2} \right)^{1/2} \frac{\partial a_{\mathrm{H}}}{\partial x}. \tag{2.12}$$

Integrating this equation across the thickness of the membrane l produces the following equation:

$$J_{\mathrm{H}} = D_M K_S \left(p^{\circ}_{\mathrm{H}_2} \right)^{1/2} \frac{a_{\mathrm{H,up}} - a_{\mathrm{H,dn}}}{l}, \tag{2.13}$$

where $a_{\mathrm{H,up}}$ and $a_{\mathrm{H,dn}}$ are the hydrogen activities within the upstream and downstream faces of the membrane, respectively. Continuing our assumption of local equilibrium at the membrane faces, we can replace the hydrogen activities with the partial pressures of hydrogen at the membrane faces to produce Richardson's equation [26, 51]:

$$J_{\mathrm{H}} = D_M K_S \frac{p^{1/2}_{\mathrm{H}_2,\mathrm{up}} - p^{1/2}_{\mathrm{H}_2,\mathrm{dn}}}{l}. \tag{2.14}$$

This equation describes the flux of hydrogen atoms across a non-porous solution-diffusion membrane (i.e., a dense palladium membrane) when both faces of the membrane are in local equilibrium with the impinging atmosphere.

By contrast, because porous membranes do not operate via dissociation of the hydrogen

molecules into individual hydrogen atoms, equation 2.10 is not used to simplify Fick's first law [26]. Therefore, in accordance with the ideal gas law, the concentration difference $C_{H_2,up} - C_{H_2,dn}$ can be replaced directly by the partial pressure difference $p_{H_2,up} - p_{H_2,dn}$, assuming that the temperature is identical on both sides of the membrane, as is usually the case. This restricts us to the use of the concentration gradient to determine the flux through porous membranes:

$$J_{H_2} = -D_M \frac{p_{H_2,up} - p_{H_2,dn}}{l}. \tag{2.15}$$

Additionally, since permeate flow through porous membranes is restricted by the porosity ϕ of the material and tortuosity τ of the pores, D_M must be replaced by the effective diffusivity [53]:

$$D_M^{eff} = \frac{\phi}{\tau} D_M. \tag{2.16}$$

Substituting this into equation 2.15 results in the following equation for diffusive flux through a porous membrane:

$$J_{H_2} = -D_M^{eff} \frac{p_{H_2,up} - p_{H_2,dn}}{l}. \tag{2.17}$$

Flux through oxide membranes, which utilize dense ceramic layers for separation, is governed by a different set of equations. In a general sense, the hydrogen flux through this type of membrane can be described by the Wagner equation:

$$J_{OH_O^{\cdot}} = \frac{1}{L}\left(\frac{RT}{4F^2}\int_{P'_{O_2}}^{P''_{O_2}} \sigma_t t_{OH_O^{\cdot}} t_{V_O^{\cdot\cdot}}\, d\ln P_{O_2} + \frac{RT}{2F^2}\int_{P'_{H_2}}^{P''_{H_2}} \sigma_t t_{OH_O^{\cdot}} \left(t_{V_O^{\cdot\cdot}} + t_{e'}\right) d\ln P_{H_2}\right), \tag{2.18}$$

where σ_t is the total conductivity of the material; t_i is the transference number of the charged species, where $i = OH_O^{\cdot}$ (a hydroxyl ion), $V_O^{\cdot\cdot}$ (an oxygen vacancy in the lattice), e'

(an electron); F is the Faraday constant; and $d \ln P_{O_2}$ and $d \ln P_{H_2}$ are the chemical potential gradients of oxygen and hydrogen, respectively [37,39,54,55]. The rate of hydrogen diffusion described by this schema is effectively doubled, as this equation describes the transport of a single proton across the membrane rather than an entire hydrogen molecule (H_2), as in equation 2.17. Under the negligible oxygen conduction condition, in which very little oxygen is transferred from one side of the membrane to the other, the Wagner equation can be simplified to the following [37,39]:

$$J_{OH_O^{\cdot}} = \frac{1}{L}\left(\frac{RT}{2F^2}\int_{P'_{H_2}}^{P''_{H_2}} \sigma_t t_{OH_O^{\cdot}} t_{e'}\, d \ln P_{H_2}\right). \tag{2.19}$$

An additional interesting property of this type of membrane is revealed by the following equation:

$$J_{OH_O^{\cdot}} \propto \sigma_{amb} = \frac{\sigma_{OH_O^{\cdot}}\sigma_{e'}}{\sigma_{OH_O^{\cdot}} + \sigma_{e'}}, \tag{2.20}$$

where σ_{amb} is the ambipolar conductivity and $\sigma_i = \sigma_t \times t_i$. Because the flux through the membrane is proportional to this ambipolar conductivity, it is important to have a material that exhibits roughly similar electronic and protonic conductivities, thereby maximizing the ambipolar conductivity.

The other defining characteristic of membranes is selectivity, which describes a membrane's ability to separate one desired component of the feed gas from another, undesired components [52]. Selectivity is always referred to as "A/B Selectivity," where A is the desired component and B is the undesired component. This property is expressed via

the retention R or separation factor α:

$$R = 1 - \frac{C_{\mathrm{H_2,up}}}{C_{\mathrm{H_2,dn}}}, \tag{2.21}$$

$$\alpha_{\mathrm{H_2/CO_2}} = \frac{C_{\mathrm{H_2,dn}}/C_{\mathrm{CO_2,dn}}}{C_{\mathrm{H_2,up}}/C_{\mathrm{CO_2,up}}}. \tag{2.22}$$

Generally speaking, retention is used for dilute mixtures, while separation factor is normally used for gas mixtures and will therefore be used for selectivity calculations in this study [56].

2.4.3 Variables Effecting Permeation

For obvious reasons, high flux and high selectivity are desired properties of membranes. Generally speaking, selectivity is an intrinsic property of the selected membrane material. Therefore, in order to maximize the output of a given membrane, it is desirable to use a highly selective material in a construction that maximizes the diffusive flux. An examination of the equations above indicate which properties and dimensions allow for the most efficient membranes.

The first and most obvious controllable factor to maximize flux through a membrane is its thickness l, shown in equations 2.14 and 2.17. When other factors are held constant, a thinner membrane will have a higher diffusive flux [29, 52]. Because of the difficulty in producing a mechanically sound membrane while simultaneously minimizing thickness, a popular membrane construction technique consists of mounting a thin selective layer onto a porous substrate, called the support layer [50]. This allows for the creation of membranes that can withstand the requisite pressure differentials and temperature swings of long-term use.

The second factor that impacts the diffusive flux of a given membrane is the difference between the square roots of the partial pressures (for non-porous membranes) or between the partial pressures (for porous membranes) of hydrogen at the up- and downstream membrane faces. In practice, this is exploited by manipulating both the total pressure difference and the rate at which permeate gas is transported away from the downstream face of the membrane. Since the mole fraction of hydrogen is generally fixed in the feed gas, increasing the overall pressure of the feed gas is the only way to affect the partial pressure difference on the feed side of the membrane. On the downstream side of the membrane, the methods by which the partial pressure difference can be modified include reducing the overall pressure and reducing the concentration of permeate next to the membrane. In some cases this is achieved by using a sweep gas to transport the permeate away from the downstream side of the membrane [57].

The final factor that affects a membrane's flux is the temperature. Although temperature does not explicitly appear in equations 2.14 or 2.17, it is present in the equations for both Sieverts' constant and the diffusion coefficient [58]. Additionally, although this is generally impractical, inducing a temperature difference between the upstream and downstream sides of the membrane is another way to modify the partial pressure differential. When considering changes to any of these factors, it is important to keep in mind the thermal and mechanical limitations of the membrane, which can vary widely based on construction method, material composition and manufacturing tolerances.

2.5 Holey Graphene

A material known as holey graphene recently gained attention as a potential hydrogen separation membrane. This material, formed by introducing holes into two dimensional graphene sheets, operates as a porous membrane via size exclusion [59]. This approach is markedly different than the solution-diffusion method utilized by current hydrogen separation membranes, and offers significant advantages in cost [11]. Holey graphene is currently being studied by several research groups, including members of the Department of Materials Science and Engineering at the University of Maryland, College Park led by Dr. Liangbing Hu.

2.5.1 Graphene

Graphene is most simply described as a single layer of graphite. While the more pedestrian graphite has been widely used in applications as varied as pencils, lubricants, electrodes, insulators, and carbon fiber composites for many years, reducing it down to the single layer structure of graphene was only accomplished recently. In the early 2000s, several methods were utilized in attempts to create ever-thinner layers of graphite, including manipulation via atomic force microscope tips and subjection of nano-sized diamonds to temperatures of 1600 °C [60]. In 2004, single layer graphene was created by using ordinary cellophane tape to remove layers of graphene from a flake of graphite and then deposit them on a surface via van der Waals attraction [61]. Once creation of these single-atom thickness films was possible, several potential uses for this novel material were quickly investigated in electronics, composites, chemical detection, among others [60, 62]. In addition, extensive efforts were undertaken to create and characterize various forms of graphene, including

bi-layer graphene (BLG), few-layer graphene (FLG), graphene oxide (GO), and reduced graphene oxide (rGO). Additional research investigated other two-dimensional materials such as transition metal oxides (TMOs), transition metal dichalcogenides (TMDs), and metal-organic frameworks [62].

2.5.2 Creation of Holey Graphene

One enticing property of graphene is that it is both infinitesimally thin and acts as a completely non-permeable material [63,64]. The discovery of these characteristics introduced the possibility of creating a porous material with controllable pore size, shape, and density, which is of significant interest in several fields. In order to do this, however, a method of introducing the pores needed to be developed. In the early 2010s, research began into the nanolithographic creation of meshes formed out of graphene with the intention of using them as semiconductors [64, 65]. These first so-called holey graphene (hG) materials were of limited use outside of electronics due to their poor scalability, however [59]. Because of this shortcoming, significant research efforts began into methods to reliably create large quantities of graphene with controllably sized pores via other methods, including steam etching, chemical activation, and catalytic or enzymatic oxidation [66]. In 2015, researchers discovered a method to create holey graphene via direct partial oxidation in air at elevated temperatures, eliminating the need for catalysts and allowing for the fine control of pore size and distribution. This method allowed for the creation of robust and dense films at relatively low cost by relying on the presence of irregular defects in the graphene lattice. These defects are the first portions of the mesh to gasify during oxidation, resulting in the

creation of pores through the thickness of the film layer, while continued oxidation enlarges the pores [66]. This distinctly two-stage pore formation process is illustrated in figure 2.6. The material produced via this process, depicted in figure 2.7, resembles a fine powder and is in the form of small (roughly 1 µm to 10 µm in lateral length) flakes of material which can be pressed in to various shapes [11].

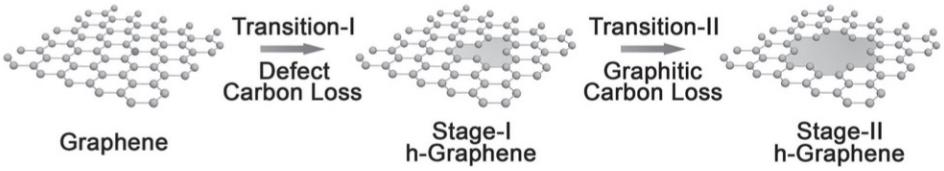

Figure 2.6: Graphene subjected to elevated temperatures in air undergoes a two-stage oxidation process, resulting first in the creation of pores at the sites of mesh defects, then the expansion of pores due to loss of graphitic carbon around their edges [66].

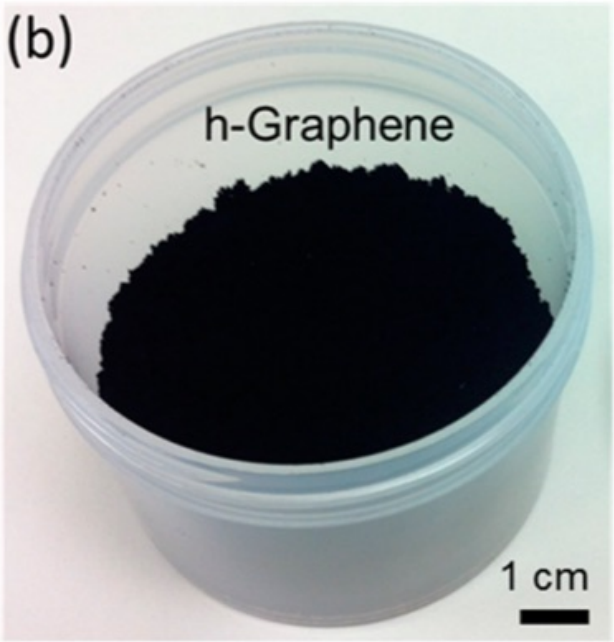

Figure 2.7: As-synthesized holey graphene powder [11].

2.5.3 Holey Graphene Properties

This novel holey graphene material differs in several important aspects from standard non-porous graphene. Holey graphene is much less dense than an equivalent amount of intact graphene flakes, which allows it to be formed into dense films by compression much more easily than intact graphene, which traps interstitial molecules between the layers and prevents the layers from adhering to each other [11,67]. This is extremely important in allowing for the creation of membranes durable enough to withstand the pressure differential necessary for gas separation. In experiments that attempted film creation via vacuum filtration, the films made using holey graphene exhibited thicknesses roughly one-fifth that of films made using intact graphene flakes at equivalent areal mass densities [11]. SEM imaging of the created films revealed that those made with intact graphene flakes were arranged in a random fashion, in contrast with the semi-regular layered arrangement of holey graphene flakes in the other set of films [11]. These unique properties make holey graphene an ideal candidate for the creation of films and membranes that are both porous and durable.

2.5.4 Holey Graphene Membrane Production

The holey graphene membranes used in this study was created by first producing holey graphene flakes, as discussed in section 2.5.2, and then compressing them into disk-shaped membranes. The holey graphene flakes were made by oxidizing pure graphene sheets in air at 430 °C for 10 hours. This material exhibited a tight pore distribution with an average pore size of 8 nm and a pore density of approximately 630/μm^2 [11]. SEM and TEM images of the pores and a plot of the pore diameter distribution is shown in figure 2.8. The flakes

were then formed into the membranes via dry pressing using a 1 in (2.54 cm) diameter die, pictured in figure 2.9, and a hydraulic press. The pores present in the holey graphene material permitted this method of construction by allowing gas molecules to escape from between the graphene flakes during compression; similar processing of pristine graphene sheets resulted in the material experiencing significant rebounding, preventing the formation of a monolithic membrane structure [68]. Copper foil was used to prevent the holey graphene from sticking to the die faces.

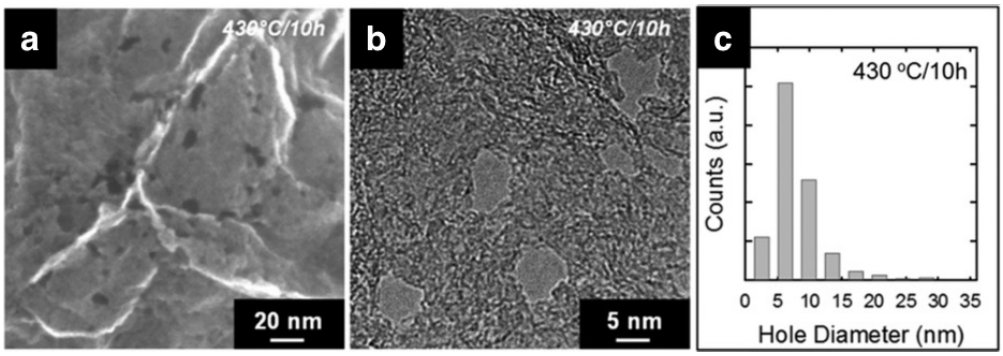

Figure 2.8: Typical SEM (a) and TEM (b) surface images, and hole diameter distribution (c), of holey graphene samples oxidized at 430 °C for 10 hours. This oxidation schema provided a relatively tight pore size distribution, although the lack of perfect pore size uniformity introduced the potential for Pouselle flow through the membrane [11].

Figure 2.9: The dry press die used to form the holey graphene membranes [69].

2.5.5 Reduced Holey Graphene

So-called "reduction" processing of holey graphene material offered one method of modifying the performance characteristics of the standard holey graphene material. During this study, this process was conducted by sandwiching pressed sheets of holey graphene between two carbon blocks and placing them in an argon-filled furnace that was heated to 1000 °C at a rate of 2 °C/min and held there for two hours before being allowed to cool naturally. The exact way in which this process modifies the material is not definitively known, but several specific changes were noted in these and other samples subjected to the process. Mass loss was noted, while carbon content increased in the sample. Some samples also exhibited thickness reduction. The pore size and arrangement distribution did not appear to undergo significant change when compared to the unreduced sample, but some SEM imaging appeared to show an increase in very small (<2 nm to 3 nm) pores [70]. It is hypothesized that the reduction process promoted the percolation of air molecules out of the membrane structure, thereby reducing interstitial space and smoothing out the interfaces between the holey graphene flakes that make up the material. This resulted in a decrease in the overall porosity of the material. SEM imaging (shown in figure 2.10) of the reduced holey graphene material revealed a more uniform surface and more regular interior flake arrangement in the reduced holey graphene membrane, lending credence to the interstitial gas removal hypothesis.

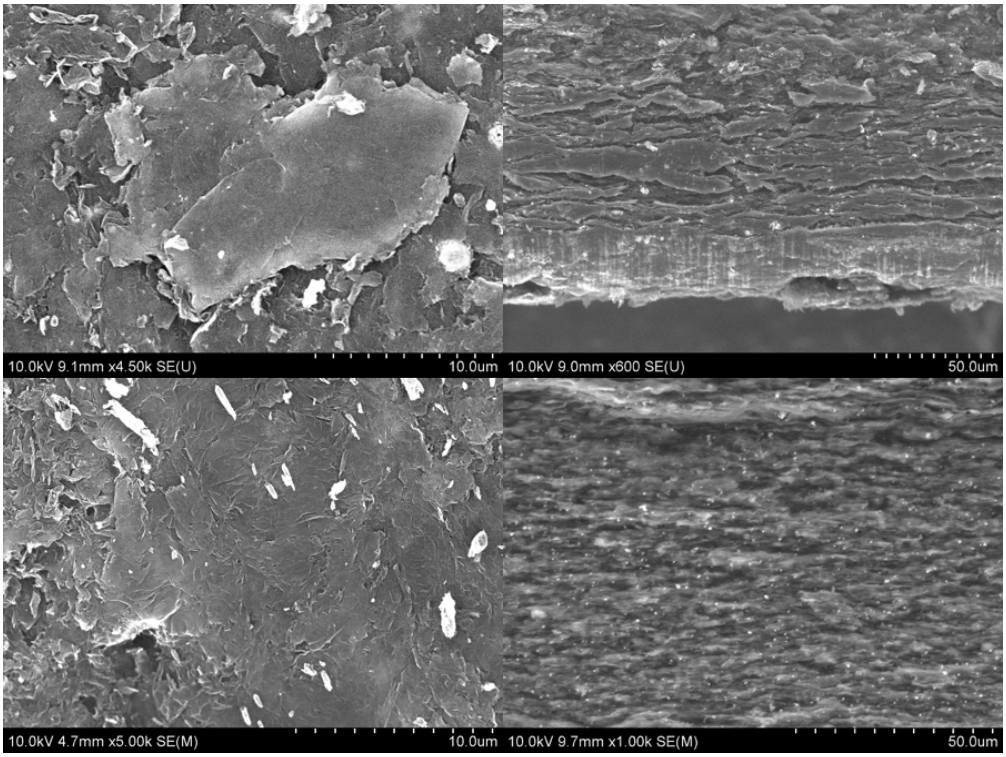

Figure 2.10: SEM imaging of the surface (left) and cross-section (right) of holey graphene (top) and reduced holey graphene (bottom) materials. Note the smoother appearance of the reduced holey graphene material [71].

2.6 Doped Perovskite Ceramics

Beginning in the early 1990s, researchers investigated using perovskite oxides as proton conductors [72–76]. Doping these oxides with multivalent cations, typically cesium and europium, allowed them to exhibit mixed (both protonic and electronic) conductivity, a requirement for selective hydrogen transport across the material [38]. These materials present significant advantages as hydrogen separation membranes, particularly with regards to cost compared to industry-standard palladium membranes [77]. Perovskite-based membranes are currently being studied by members of the Department of Materials Science and Engineering at the University of Maryland, College Park, led by Dr. Eric Wachsman.

2.6.1 Perovskite Oxides

Perovskite oxides are a family of minerals with a crystal structure (illustrated in figure 2.11) of ${}^{\mathrm{XII}}A^{2+}{}^{\mathrm{VI}}B^{4+}X_3^{2+}$ with oxygen at the face centers; i.e., the X designator [78]. The perovskite name comes from the first mineral in which this crystal structure was observed, $CaTiO_3$ [79]. In these materials, the A cation is a large basic ion, associated and located at the edge of the octahedral crystal structure, while B is a smaller tetravalent cation positioned in the center of the octahedron. In addition to the standard ABO_3 perovskites, there are also so-called perovskite-like minerals of the form A_2BO_4, as well as complex perovskites with formulas of $A_2B'B''O_6$ or $A_3B'B''{}_2O_9$. In many cases, all of these mineral classes are referred to simply as perovskites [38, 80, 81]. Diagrams of the ideal structure of some of these materials are shown in figure 2.11. Perovskites include minerals that exhibit several desirable characteristics, such as dielectric properties, electrical superconductivity,

and catalytic activity. The chemical stability of perovskite structures allows for the creation of a wide array of compounds, opening the door for materials tuned to specific uses [82].

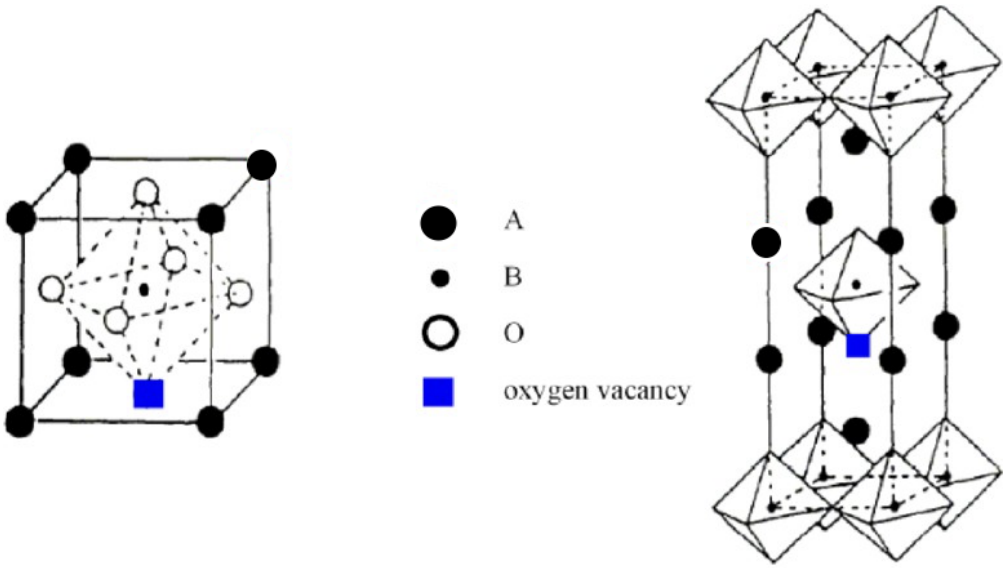

Figure 2.11: Models of ABO_3 (left) and A_2BO_4 (right) perovskite structures. A denotes a large cation, while B is a smaller tetravalent cation. O denotes an oxygen atom. Doping occurs when some of the B ions are replaced with an alternative element [80].

2.6.2 Doping of Perovskite Oxides

Although the perovskite family contains a wide variety of compounds, oftentimes specific applications call for a mix of properties that is not found in materials adhering to the standard ABO_3 formula. To remedy this, a process called doping is utilized to modify the characteristics of these materials by replacing a certain percentage of the tetravalent B cations with various trivalent or mixed +3/+4 valency cations. This doping has been performed on several different perovskites, including strontium cerate ($SrCeO_3$) and barium cerate ($BaCeO_3$). Different dopants have different effects on the properties of the base material, allowing for the creation of compounds specifically designed to address

a wide variety of operating conditions and performance requirements. Common elements for use as dopants include europium, gadolinium, neodymium, praseodymium, samarium, ytterbium, thulium, yttrium, and zirconium [34,38,83]. For example, researchers discovered that doping with zirconium increased the chemical stability of strontium cerate, while doping with europium increased its electronic conductivity [38,84]. This was an important discovery because, while undoped strontium cerate had attracted interest in the field of hydrogen separation due to its high protonic conductivity and its stability in temperatures up to 1000 °C, its electronic conductivity was deemed too low to be an efficient hydrogen separation [85]. During the doping process, the chemical formula of the perovskite material is modified to the form $AB_{1\text{-}x}M_xO_{3\text{-}x/2}$, where M represents the dopant element and x indicates the atom percentage of doping. Doping can also be performed with multiple dopants. In these cases, the chemical formula is of the form $AB_{1\text{-}(x+y)}M_xM'_yO_{3\text{-}(x+y)/2}$. In most cases, $x(+y) < 0.3$ due to mechanical stability concerns [36, 38, 75]. Introducing a lower-valency cation (referred to as "acceptor doping") to the B site induces oxygen vacancies ($V_O^{\cdot\cdot}$ in Kröger-Vink notation) in the material [83]. Protons can then be incorporated into the lattice structure through two mechanisms; either attaching to an oxygen lattice site ($O_O^{\times}$) or, along with an oxygen atom, forming a hydroxyl ion ($OH_O^{\cdot}$) and occupying an oxygen vacancy [83,86–88]. The reaction for this process, which shows both possibilities, is

$$H_2 + \frac{1}{2}O_2 + V_O^{\cdot\cdot} + O_O^{\times} \longrightarrow 2OH_O^{\cdot}. \tag{2.23}$$

Based on the above equation, if the feed gas does not include any oxygen with which to create hydroxyl ions, hydrogen atoms are limited to transiting across the membrane via attachment

to existing oxygen lattice sites. This occasionally results in the desorption of an entire hydroxyl ion to form a water molecule on the downstream side of the membrane, leading to a decrease in hydrogen transport across the membrane over time due to a dearth of available oxygen lattice sites to which the hydrogen atoms can attach $\mathrm{Oh}-2009\,\mathrm{ac_Oh}-2008\,\mathrm{aa}$. By contrast, if oxygen is available in the feed gas (almost exclusively in the form of water vapor), transit through the membrane via an oxygen vacancy is also available [83,86,88]. Because of this fact, adding water to the feed side gas is a cheap and effective way by which hydrogen production can be increased using these membranes.

2.6.3 Creation of Doped Perovskites

Because perovskites are stable at high temperatures and are also stable in terms of thermodynamic equilibrium, they can only be produced at high temperatures (generally higher than 1000 °C) and with long calcination times, usually in excess of 10 hours [37, 39, 80, 82]. The synthesis process itself is simple, consisting of direct annealing of the appropriate mixture of metal oxides at elevated temperatures. Because the perovskite is produced directly from the constituent oxides, no toxic gases are created in the process, making the manufacturing of these materials relatively environmentally friendly. However, because of this, tolerances in ingredient purity, ratios, and homogeneity are extremely strict. Ball milling is used to ensure the components are well-mixed prior to annealing [80]. Once the perovskite material was been created, it could be manipulated into many different structures via methods such as tapecasting, grinding, colloidal coating, or pelletizing [35,39,75].

2.6.4 Doped Perovskite Membrane Production

The doped perovskite membranes researched during this study were dense tubular membranes manufactured in a multi-step process that produced a hollow tube, capped at one end, with a dense selective layer coated on the interior surface of a porous, mechanically supportive diffusive layer. The manufacturing process began with the creation of a $NiO-SrCeO_3$ metal oxide-perovskite slurry via ball milling the ceramic powder, metal oxide powder, ethanol, and toluene together. Polyvinyl butyral (PVB, a resin used as a binder) and benzyl butyl phthalate (BBP, a plasticizer used to lower the glass transition temperature of the PVB) were then added to the mixture, which was degassed to remove any air bubbles from the mixture. A tape casting machine was then used to form the material into a thin, uniform sheet roughly 600 µm thick. The sheet was allowed to partially dry before cutting it into sections; coating the sections with an adhesive consisting of ethanol, PVB, and BBP; and rolling them onto steel mandrills to form hollow tubes of the substrate. Separately, several small pieces of the substrate were stacked and compressed in a hydraulic press to form material for the tube end caps. Once the tubes had dried fully, they were removed from the mandrills and one end was sealed using the previously formed end caps and additional adhesive. The tubes were then pre-sintered at temperatures of 1100 °C to 1200 °C in order to set the binder and remove the plasticizer. Concurrently with the creation of the tubular porous supports, a slurry of the dense doped perovskite selective layer was created via the conventional solid state reaction process, whereby strontium cerate was ball-milled with oxides of the various B-site cations in the desired stoichiometric ratios for at least 24 hours and then calcined in air. This slurry was applied to the interior of the tubular support via

colloidal coating and the entire assembly was then co-sintered.

2.6.5 Doped Perovskite Membrane Experimental Suitability

After reviewing the properties of the dense perovskite oxide membranes, it was readily apparent that this style of membrane was well-suited for use in the separation of hydrogen from a mixture of gases. Perovskite membranes exhibit high hydrogen flux and high selectivity; operate at temperatures of 700 °C to 900 °C, roughly equivalent to the temperatures at which biomass gasification is conducted; and can be used in setups that incorporate WGS and carbon dioxide reforming of methane (CDRM) to increase hydrogen yields by selectively removing hydrogen from the reaction side of the membrane throughout the reaction process, shifting the equilibrium points of the reactions [36, 39, 77, 84, 85]. However, concerns related to the experimental setup precluded the use of these membranes in this study. The necessary operating temperatures for the perovskite membranes far exceed the design parameters of the experimental facility and raised the possibility of serious damage to the components of the facility, particularly the tubing and connecting fittings. An ancillary concern centered around the chemical stability of the particular perovskite lattice investigated for use in this study. The specific membrane composition analyzed for use in this study was 5% and 10% praseodymium-doped strontium cerate, which has the chemical formula [89]:

$$\mathrm{SrCe_{1-x}Pr_xO_{3-x/2}} \quad (x = 0.05, 0.1). \tag{2.24}$$

Because this particular membrane is doped using only praseodymium, when carbon dioxide is present in the feed gas, the perovskite lattice (simplified to its undoped form in this formula) interacts with it according to the following reaction in order to form cerium oxide and strontium carbonate [84]:

$$SrCeO_3 + CO_2 \longrightarrow SrCO_3 + CeO_2. \tag{2.25}$$

This effect can be mitigated with zirconium doping in order to decrease the material's basicity and increase its chemical stability, but zirconium-doped membranes were not available for testing. Because of these concerns, the decision was made to not conduct testing using the dense tubular perovskite membranes.

2.7 Prior Experimentation

Aside from membrane selection and preparation, it is equally important to create a membrane housing that can hold the membrane and withstand the potentially caustic gases, elevated pressures, and high temperatures present in gas separation operations. It is of vital importance that this housing prevent any leaks, both across the membrane and into or out of the gas separation system as a whole. It is of utmost importance that the housing be able to support the membrane in such a way as to maximize exposure of the selective layer to both the feed and sweep gases. This allows for the highest possible diffusive flux across the membrane.

In addition to the housing itself, the design of the experimental setup as a whole also has a significant impact on the effectiveness of the gas separation operation. It must

be designed to accommodate both the membrane and its housing, and must include all components necessary for control of the experiment. These components include flowmeters, valves, pressure and temperature gauges, heat sources, and gas analyzation equipment.

2.7.1 Membrane Housing Development

Membrane housings, in general, are designed to accommodate one of two major membrane styles: tubular or disk. These two membrane styles have rather self-explanatory construction. Tubular-type membranes are cylindrical in structure and can have either one or two open ends. In the case of single-ended tubular membranes, a concentric tube is inserted into the open end to provide for proper gas circulation through the membrane, as shown in figure 2.12. This style of membrane allows for a large selective layer area within a relatively small footprint, as well as increasing the time of feed gas contact with the membrane surface as it flows along the length of the membrane. Conversely, these membranes are somewhat more time-consuming to manufacture than disk-style membranes.

Obviously, membrane housing design for a specific experiment reflects the design and limitations of the chosen separation membrane. This results in a wide variety of membrane housing designs that nevertheless exhibit several shared features. One very early design for separating gases was patented over 100 years ago by Walter Snelling, and consisted of a casing bisected along the long axis by a porous partition atop which a layer of impermeable palladium or platinum was deposited. Snelling also patented various styles of housings that incorporated an inner tube inside the outer housing that takes the place of the partition mentioned above [27]. Representative examples of these housings are shown in figures 1

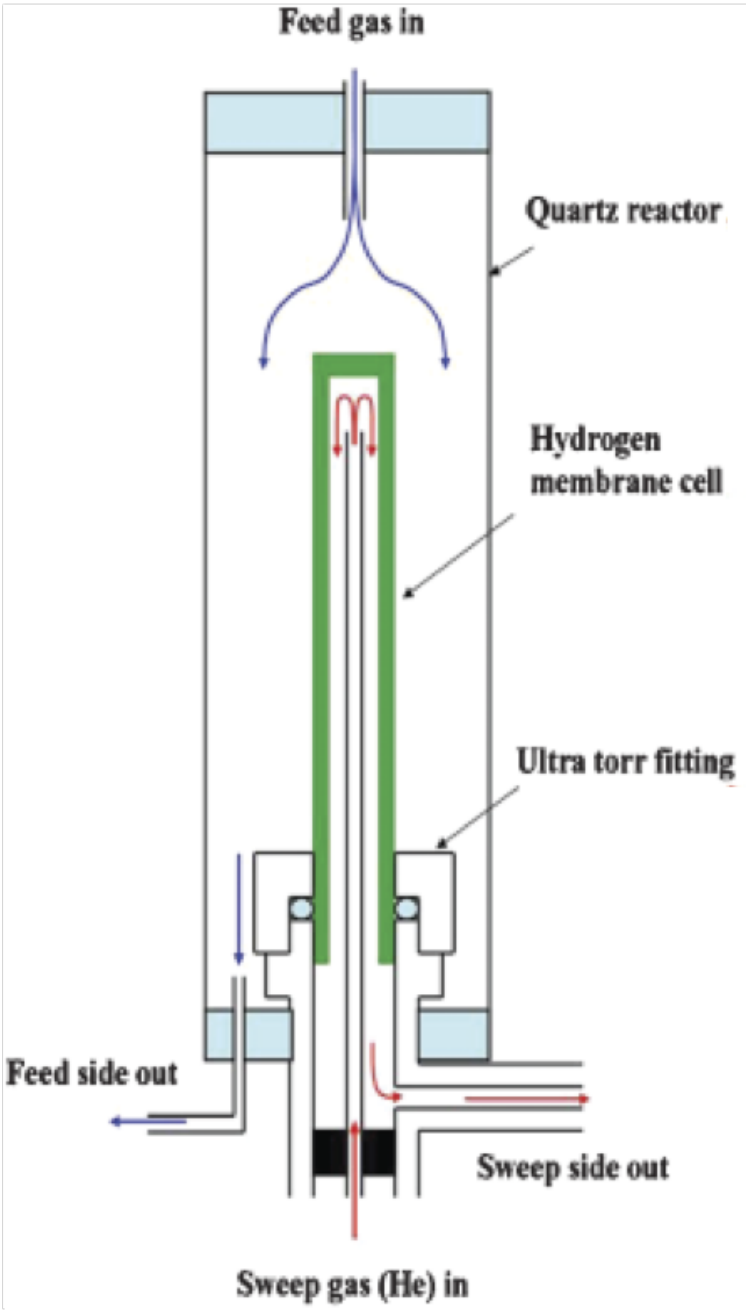

Figure 2.12: General schematic of the operation of a tubular membrane, shown in green. Note the flow of sweep gas indicated by the red arrows [35].

and 2 of figure 2.13, respectively. The gas to be separated is introduced to the housings at an elevated pressure through tubes (10, 18) and flows along the selective layers (9', 17). Hydrogen is diffused across the membranes into the outer chamber and exits via the outlet pipes (11, 21). Undiffused retenate exits the housing via tubes (12, 19). These housings also incorporated heating elements in the porous partition, denoted by (14/15, 23/24), to mitigate the risk of hydrogen embrittlement of the selective layer mentioned previously. Preferably, these heating elements maintained the casing and enclosed gas at a temperature in excess of 800 °C, although this could be varied to some degree [27].

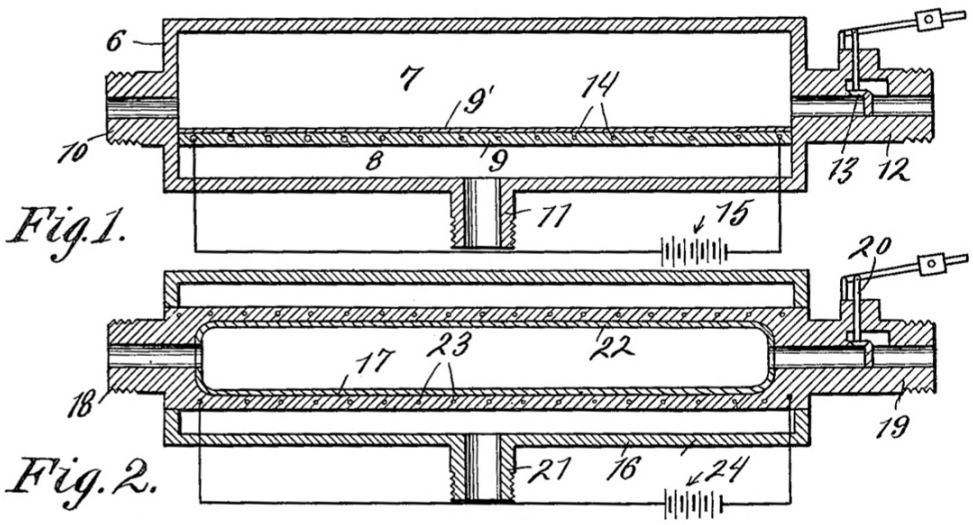

Figure 2.13: Two gas separation housings designed and patented by Walter Snelling. Components 9' and 22 are the selective layers of the membranes, while components 9 and 17 are the mechanically supporting diffusive layers [27].

A later membrane housing design, which utilized a disk-type membrane, was patented by Makrides et al. in 1967. A representative schematic of this style of membrane housing is shown in figure 2.14. Feed gas enters the housing via the inlet pipe (18) at an elevated pressure P_1 and flows toward the membrane (10), which is composed of a group V-B metal coated in palladium or a palladium alloy. This membrane is attached to the inner tube

(12) via electron beam welding to ensure it can withstand the pressure differential $P_1 > P_2$ necessary to support diffusion. Hydrogen permeates through the membrane into the downstream side of the housing and exits via the outlet pipe (20). Often the downstream side of the membrane is attached to a pump to remove permeate from the membrane face and maintain the required hydrogen partial pressure differential. Retenate that is excluded by the membrane is diverted out of the housing through the exit pipe (22). At the bottom of the housing, valve (24) acts as a pressure and flow controller. Similar to the housings developed by Snelling 50 years before, the housings used by Makrides incorporated a heating element (26) to maintain the system at the requisite temperature. Alternatively, the entire apparatus can be heated via convective heat transfer from the feed gas [90].

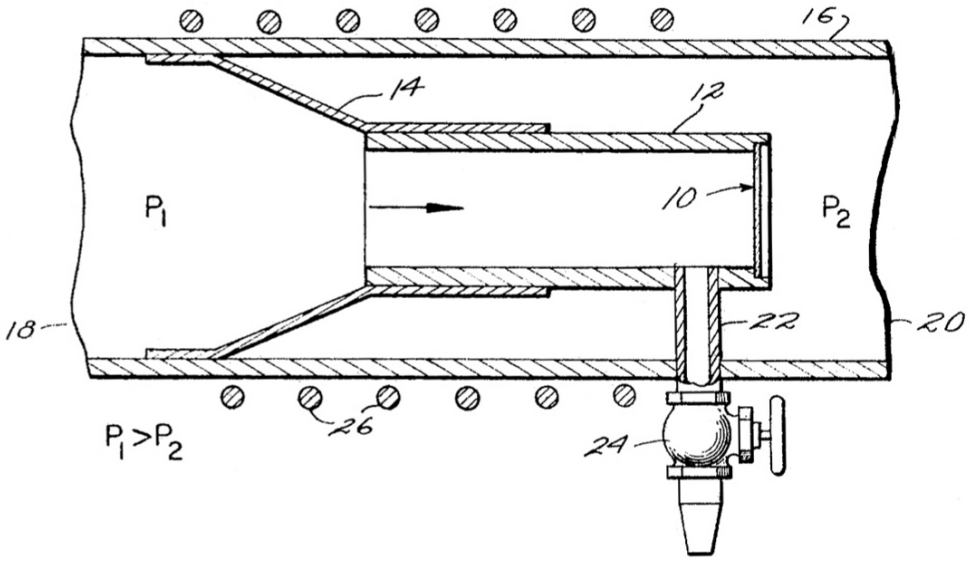

Figure 2.14: Hydrogen separation housing created by Alkis Makrides et al.; one of the first membrane housings to incorporate a disk-style membrane. Component 10 is the separation membrane; gas diffuses through the membrane from left to right [90].

These two membrane housing designs influenced subsequent hydrogen separation housing designs, most of which maintained the same general arrangement. One significant

addition in later housing designs was the use of a sweep gas across the permeate side of the membrane. Several different sweep gases have been used in prior experimentation, including nitrogen, argon, and steam. It is important that the sweep gas be inert and easy to separate from the hydrogen permeate later in the process. For this reason, steam is particularly favored in applications where the hydrogen must be used later. Use of a sweep gas has the effect of increasing the hydrogen partial pressure differential, and therefore the diffusive flux, across the membrane without increasing the overall pressure of the system This is an important consideration when dealing with membranes that lack high mechanical strength [91, 92]. An example created by the National Energy Technology Laboratory (NETL) of a housing with this setup for a disk-type membrane is shown in figure 2.15. The use of an inert sweep gas can also allow the membrane to be brought up to experimental temperature in a non-reacting atmosphere, if there is a mechanism to introduce the sweep gas to the feed side of the membrane as well. This prevents embrittlement of the membrane by hydrogen at temperatures below 300 °C [93].

Aside from holding the membrane securely and managing the flow of feed, retenate, permeate, and sweep gases, the membrane housing must ensure that leaks do not affect the diffusion of hydrogen through the membrane. Current hydrogen separation membrane technologies allow for extremely high selectivity ratios, but the presence of leaks can negate the entire separation process. In order to prevent leaks, consideration must be given not only to the housing's performance at ambient temperature, but also at operating temperature. Thermal expansion rate differences can particularly cause problems at interfaces between the housing and the membrane itself, and must be given specific attention. During their initial research into hydrogen separation, Ilias et al. encountered significant leaks from

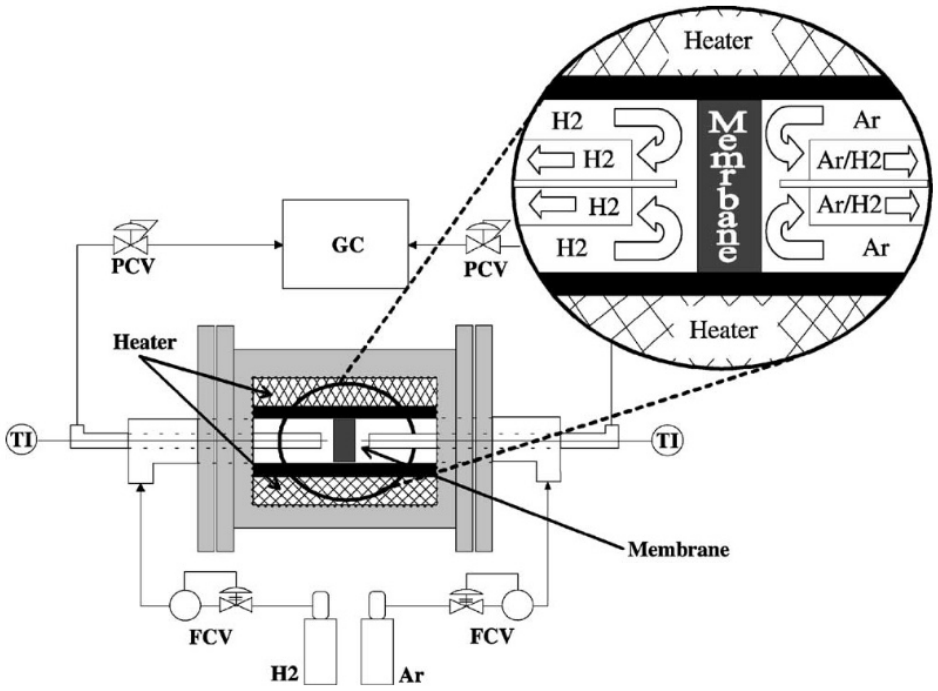

Figure 2.15: Schematic of a hydrogen separation housing utilizing a sweep gas created by NETL. Ultra-high purity argon was introduced to the permeate (right) side of the membrane and transported hydrogen away from the membrane [92].

their housing at elevated temperatures. They addressed this by changing to a self-sealing housing constructed with copper and graphite seals. With this update, no further leakage was observed [94].

A final consideration to take into account when designing a membrane housing is physical access to the membrane itself. In many cases, experimental work involves the use of multiple membranes in a range of configurations. In order to facilitate this, it is desirable to have a membrane housing that can easily be disassembled to replace the membrane quickly and without damage.

2.7.2 Experimental Setup Development

After a suitable membrane housing has been developed and fabricated, the remainder of the experimental apparatus must be assembled. This includes gas flow control, heating elements and gas analyzation equipment. Ilias et al. utilized the setup illustrated in figure 2.16. The membrane, enclosed in the separation housing, was placed in a tube furnace and connected to stainless steel inlet and outlet lines. Gauges monitored the feed and sweep gas pressure, as well as the differential pressure across the membrane. Flow rates were monitored at the inlet and outlet of the feed and sweep sides. Sample ports were included at several points throughout the system to allow for detailed monitoring of gas composition at each step of the separation process. One significant drawback of this setup was the inability to continuously monitor the gas composition, as samples needed to be extracted from the system using a syringe [94]. This decreased granularity of measurements and increased the labor required to run experiments.

A different, more complex apparatus was developed by Gielens et al. while investigating the effects of steam and carbon dioxide on hydrogen diffusion through palladium membranes. This setup, illustrated in figure 2.17, allowed for multiple feed gas compositions of various ratios of hydrogen, helium, carbon dioxide, and steam. nitrogen was used as the sweep gas in this setup. Flow rates for the gases were controlled by mass flow controllers, and a HPLC pump controlled the flow of demineralized water used as a steam source. Again the membrane was placed in a furnace, and various pressure and temperature gauges allowed for the monitoring of the system parameters. In this apparatus, a sample point included in the sweep side outlet pipe allowed for continuous monitoring of the permeate composition [95].

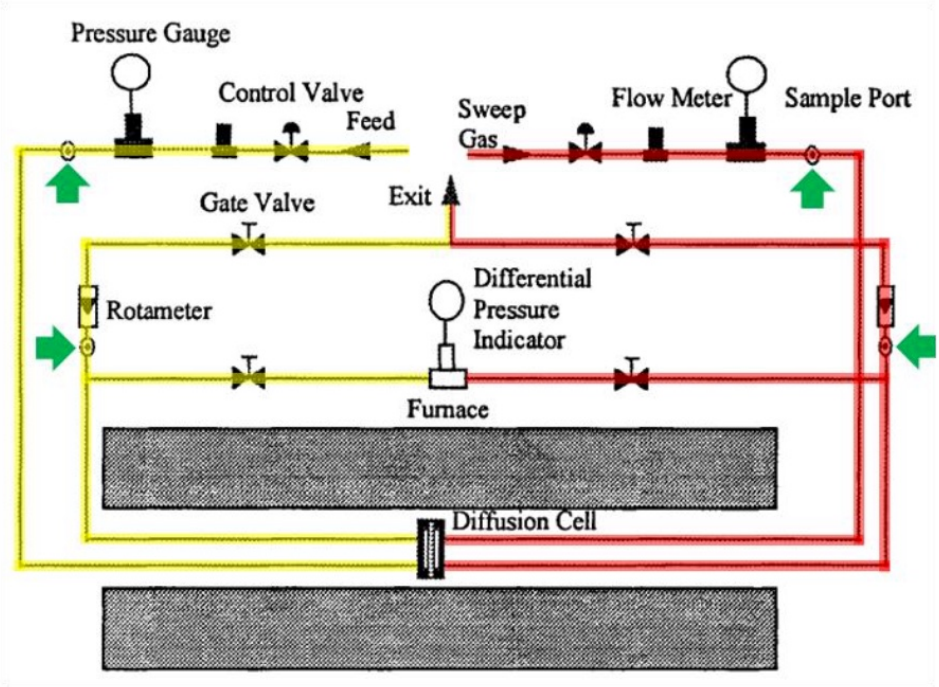

Figure 2.16: Hydrogen separation experimental apparatus utilized by Ilias et al. The feed side is shown in yellow, sweep side in red. Green arrows indicate sample ports [94].

Both of these experimental setups share many common design aspects, as do all apparatuses designed for hydrogen separation experimentation. However, unique characteristics have been incorporated into each design because of the differing objectives of their respective research teams. It is important to ensure that experimental facilities both reflect the objectives of the research and allow for modification to respond to changing research goals.

2.8 Conclusion

In the more than one hundred and fifty years since the discovery of platinum's ability to absorb and diffuse hydrogen, advances in the field have in large part focused on incremental improvements. The majority of current membrane-based research continues to center on

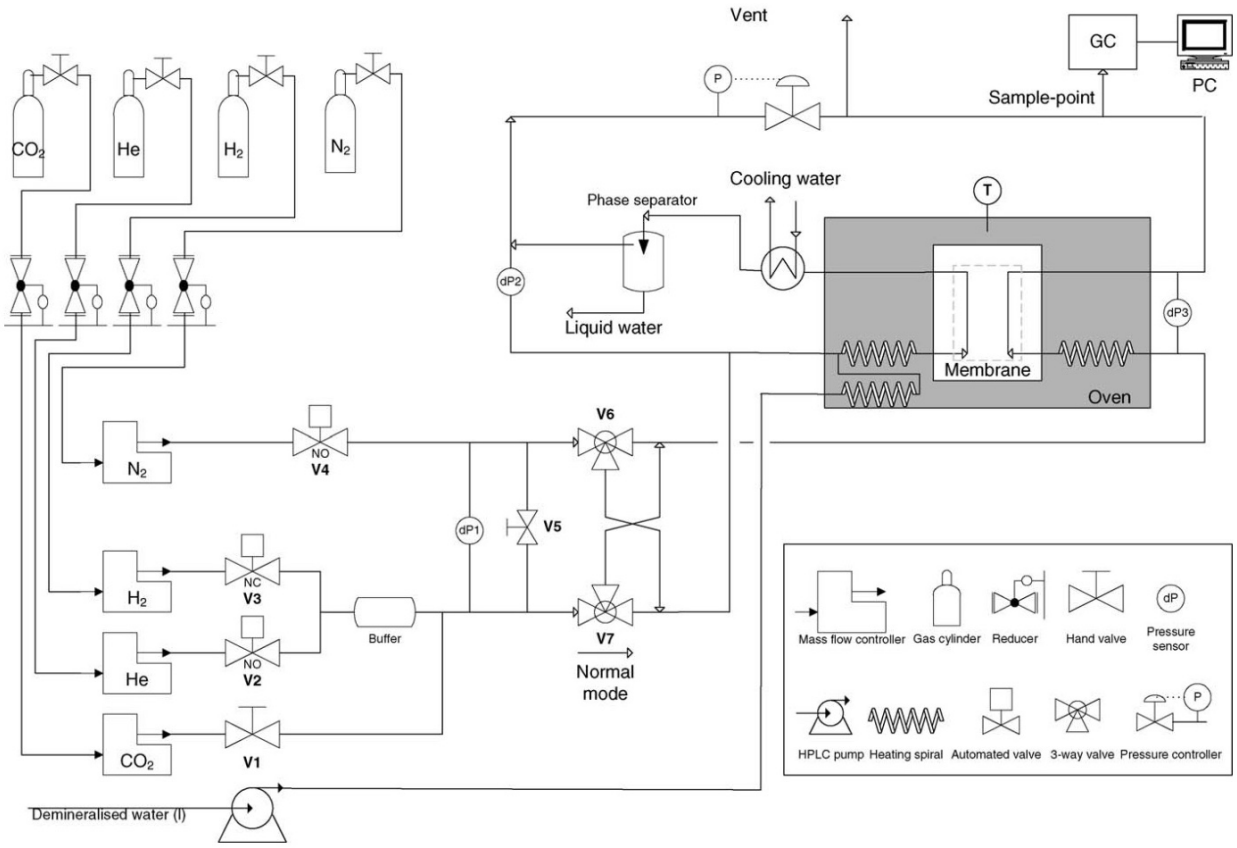

Figure 2.17: Hydrogen separation experimental apparatus used by Gielens et al. This setup allowed for continuous monitoring of the permeate gas [95].

palladium and palladium-alloy membranes, though there has been some recent research into perovskite ceramic-based membranes, and a new porous carbon material called holey graphene shows significant promise. The effectiveness of these membranes is based not only on the material's inherent diffusivity and thickness, but also the conditions under which they are used. Temperature, partial pressure of hydrogen, and composition of the feed gas all affect the hydrogen flux through the membrane. Additionally, the housing in which the membrane is mounted can have significant effects on the system's performance. Together, all of these elements influence the effectiveness of a hydrogen separation membrane. With all of these factors taken into consideration, an experimental apparatus was designed and constructed and a testing plan was developed for an investigation into the efficacy of both disk-type holey graphene membranes and tubular-type doped perovskite-based membranes for hydrogen separation.

Chapter 3: Experimental Setup

3.1 Membranes

Two distinct types of hydrogen separation membranes were investigated in this study, both of which originated from research groups at the University of Maryland, College Park. While both of these membrane types were designed to separate hydrogen from a mixed feed gas, they differed significantly in material, operating principle and configuration.

3.1.1 Holey Graphene Membranes

The first type of membrane studied was a disk-type holey graphene membrane prepared by Steven Lacey, a PhD candidate working with Dr. Liangbing Hu in the Department of Materials Science and Engineering at the University of Maryland, College Park. Multiple specimens were produced with varying properties. The general fabrication process for each specimen followed the steps outlined in section 2.5.4, but in some instances the production parameters were changed to study the resultant effects. For instance, one studied membrane (membrane 4) was sandwiched between two films of Celgard® 2325 battery separator material, some of the membranes were subjected to a reduction process as detailed in section 2.5.5, a few of the membranes were formed using different manufacturing pressures,

Table 3.1: Holey graphene membranes tested in this study.

Nbr	Mass (mg)	Thickness[a] (mm)	Mfg. Pres. (kN)	Notes
1	44.7	0.14	36	
2	61.0	0.19	36	
3	87.0	0.27	36	
4	60.0	0.26	36	Celgard Separators
5	60.0	0.22	36	Reduced
6	74.9	0.24	36	
7	59.3	0.16	70	
8	60.3	0.21	36	Reduced
9	60.0	0.40	36	Reduced, Pd-Loaded

[a] thickness measurements are based on average membrane thickness and density calculations.

and one was loaded with palladium nanoparticles using a thermal reduction process. Table 3.1 lists the holey graphene membranes investigated during this study.

3.1.2 Doped Perovskite Membranes

The second type of membrane investigated during this study for their suitability in hydrogen separation was a tubular dense perovskite membrane being researched by Mann Sakbodin and Eugene Ostrovskiy, members of Dr. Eric Wachsman's research team in the Department of Materials Science and Engineering at the University of Maryland, College Park. An example of this type of membrane is shown in figure 3.1. The original intent of this research was to compare the performance of this membrane type with that of the holey

graphene membranes mentioned above. However, after reviewing the material properties and operating principles of the dense perovskite membranes it was determined that the limitations of the experimental apparatus precluded their use in this study, as discussed in section 2.6.5. Because of this, the decision was made to forgo hydrogen separation testing using the perovskite membranes and move forward with separation experiments conducted using holey graphene membranes only.

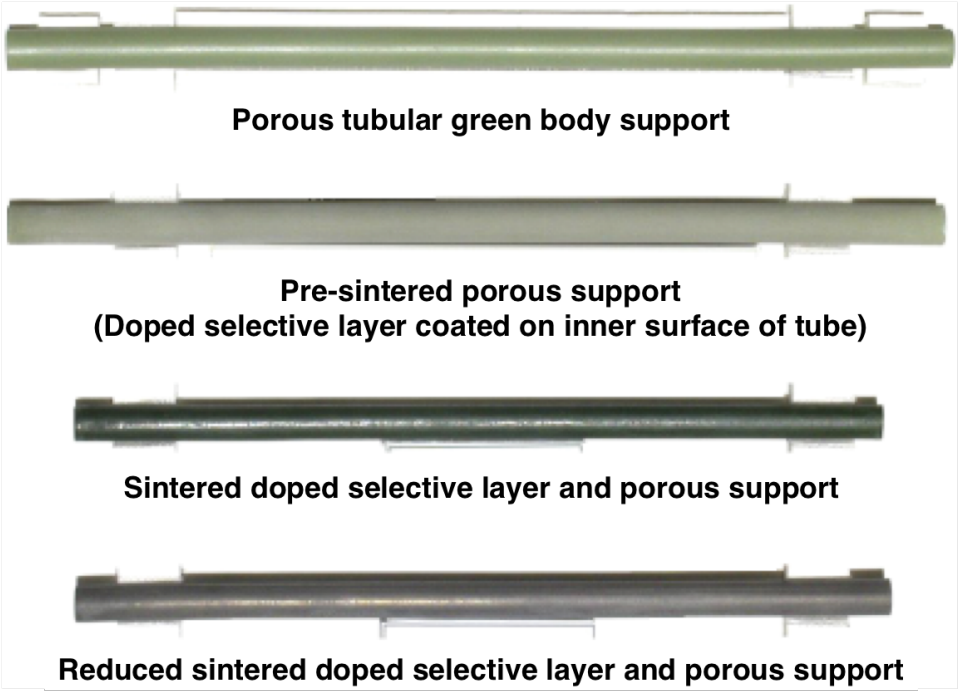

Figure 3.1: Steps involved in the production of tubular dense perovskite membranes [35].

3.2 Membrane Housing and Experimental Apparatus

This study utilized a membrane housing and experimental setup first designed and created by Ryan James and modified by Aaron Leyko, both members of the University of Maryland, College Park Combustion Lab. Minor modifications were made to the membrane

mounting point in order to accommodate the more fragile holey graphene membranes. Additionally, changes were made to the gas flow path to simplify pressure control and streamline sample collection.

3.2.1 History

The membrane housing was originally designed to withstand the environment required for experimentation using palladium-based hydrogen separation membranes. Because of their susceptibility to hydrogen embrittlement at low temperatures, the housing needed to withstand both elevated temperatures and high pressures while maintaining a seal around the membrane to prevent leakage. To this end, the housing was constructed in two halves—an upstream feed side and a downstream sweep side—that could be flanged together, holding the membrane in place and forming a tight seal while also allowing for easy access to swap membranes as necessary [7]. The two halves each have a gas inlet and gas outlet fitting, which allow for the flow of feed, retenate, sweep and permeate gases. The two halves, though they share similar exterior configurations, have significantly differing interior constructions due to the differing gas flow requirements, as shown in figure 3.2. The feed half of the housing is constructed with a cylindrical insert centered in the bored-out housing shell. With this configuration, the feed gas flows directly at the center of the membrane before being diverted radially outwards along the face of the membrane and flowing out the annular cavity and exiting through the feed gas outlet fitting. In contrast, the sweep side of the membrane consists of a solid shell with two parallel boreholes for the sweep gas and sweep/permeate gas mixture, along with a centerline borehole for a thermocouple. This induces the feed gas

to flow across the membrane, helping to move the permeate gas away from the membrane and maximize the partial pressure differential between the two sides of the membrane [6]. Copper gaskets were inserted into both the feed and sweep sides of the housing to provide a smooth mating surface for the membrane mounting gaskets.

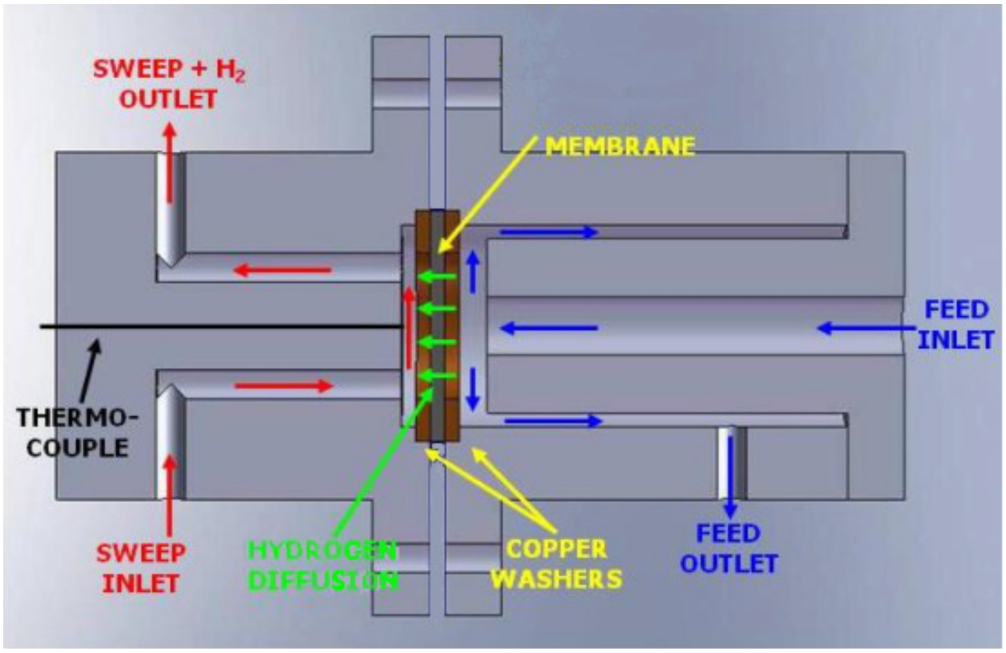

Figure 3.2: Cross-section schematic of the membrane housing [6].

In designing the feed side of the membrane housing, James needed to contend with competing goals regarding the shape of the feed chamber. The design that was settled on created a feed side exposure volume of 631 mm^3 and a surface area to volume ratio of roughly 0.31. On the one hand, a smaller surface area to volume ratio would result in less feed gas passing over the surface of the membrane. Conversely, an increase in this ratio—while allowing more feed gas to pass over the membrane surface—might lead to flow restrictions and excessive pressure inside the membrane housing [7]. The sweep side of the membrane has a smaller cavity volume due to the lower flow rate compared to the feed gas flow rates. Based on the experimental requirements, type 303 stainless steel was selected as the housing

material for its machinability, heat tolerance, and corrosion resistance. After all of the housing parts were machined, the feed side insert was welded in place and 1/8 in (0.32 cm) Swagelok® fittings were welded into place at the feed and sweep gas inlet and outlet ports, as well as the thermocouple port. Figures 3.3 and 3.4 depict the above-discussed features as well as the general arrangement of the housing.

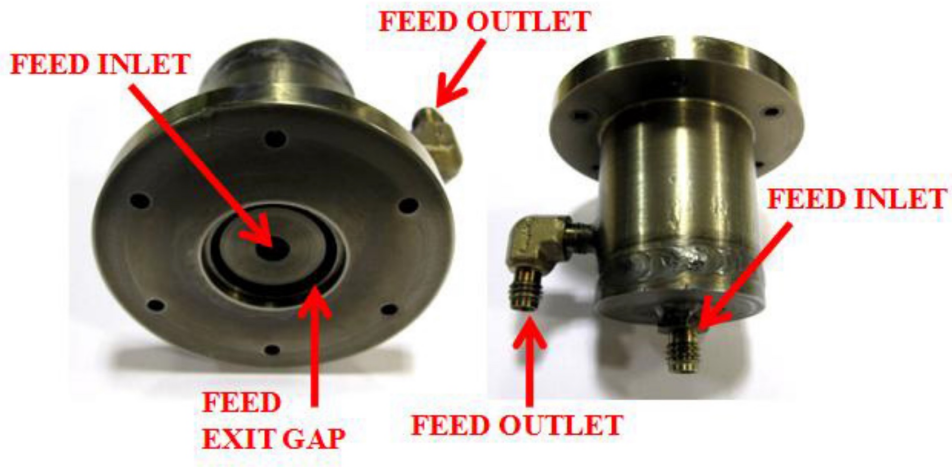

Figure 3.3: Images of the membrane housing feed side, showing the inner (left) and outer (right) arrangements. Note that the interior copper washer is not installed [6].

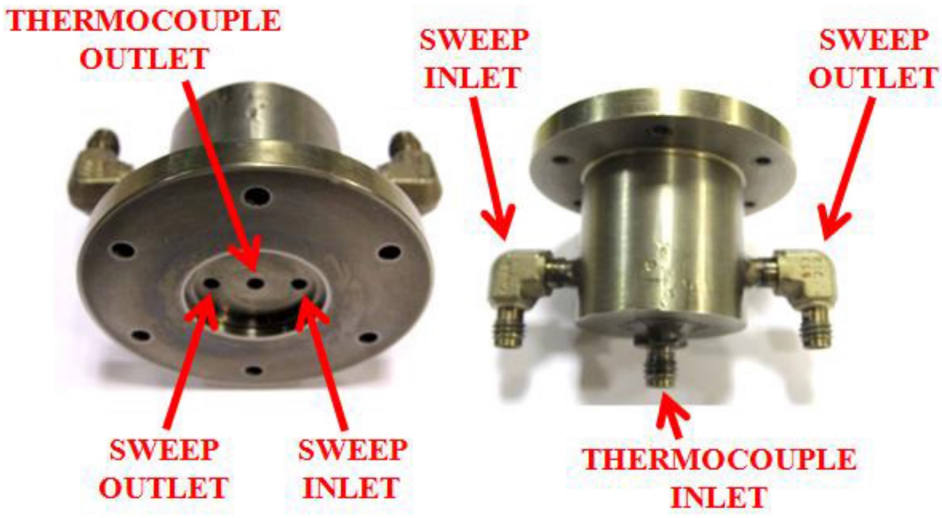

Figure 3.4: Images of the membrane housing sweep side, showing the inner (left) and outer (right) arrangements. Note that the interior copper washer is not installed [6].

To assemble the membrane housing for testing, the two halves were connected using six 5-40 machine screws tightened to roughly $0.5\,\mathrm{N}\cdot\mathrm{m}$. This low torque specification was due to the small size of the machine screws used, the construction of the membrane holder, discussed below, and the fragility of the holey graphene membranes. The assembled membrane housing was then attached to the feed and sweep gas lines to prepare for experimentation. Figure 3.5 depicts the membrane housing fully assembled and ready for testing.

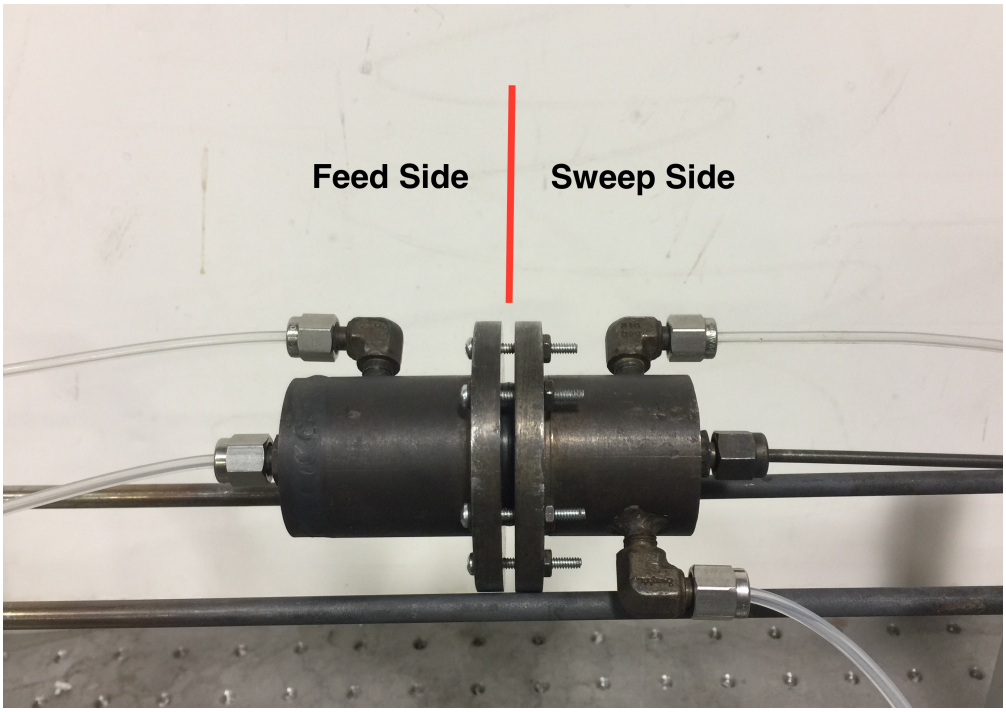

Figure 3.5: The membrane housing fully assembled and ready for testing.

A second housing was constructed in the earlier stages of the study in anticipation of testing the tubular perovskite membranes. This housing mirrored the general arrangement of the housing used by Yoon et al. and depicted in figure 2.12. Minor changes were made to the sweep gas inlet and outlet fittings, but in other respects the arrangement of the housing was essentially identical, as can be seen in figure 3.6. This housing was made of type 304 stainless steel, chosen for its corrosion resistance and machinability, with type 316 Swagelok fittings.

Schedule 40 piping was used for structural robustness and ease of fabrication. A threaded connection between the outer housing and the cap enabled easy access to the membrane itself while also allowing for a gas-tight connection using thread sealant. The stack of fittings on the right-hand side of figure 3.6 allows for the feed gas to flow from right to left down the thin white alumina tube to the far end of the tubular membrane before reversing direction and flowing back down the length of the membrane, into the thicker silver steel tube surrounding the alumina one, and out the feed outlet fitting. This maximizes the interaction time between the feed gas and the membrane surface while also ensuring a constant flow of new feed gas along the surface of the membrane. As discussed earlier, however, this housing was not used in experiments due to the factors mentioned in section 2.6.5.

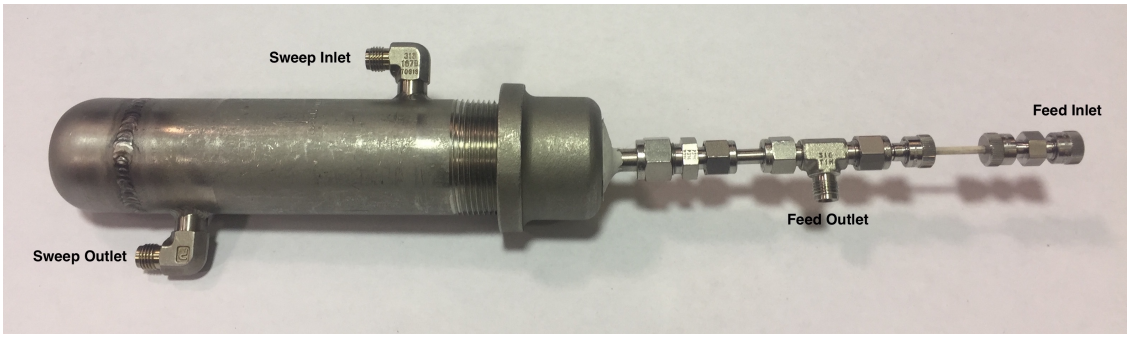

Figure 3.6: Housing designed by the author and constructed by the University of Maryland Aerospace Engineering Machine Shop during this study for use with dense tubular perovskite membranes.

3.2.2 Experimental Apparatus

The experimental apparatus used in this study mirrored many of the arrangements found in prior literature. At its most basic level, the apparatus consisted of flow controllers to manage the flow rates of both feed and sweep gases, valves to both direct the gas flow and manage the system pressure, gauges to monitor the conditions within the system, a

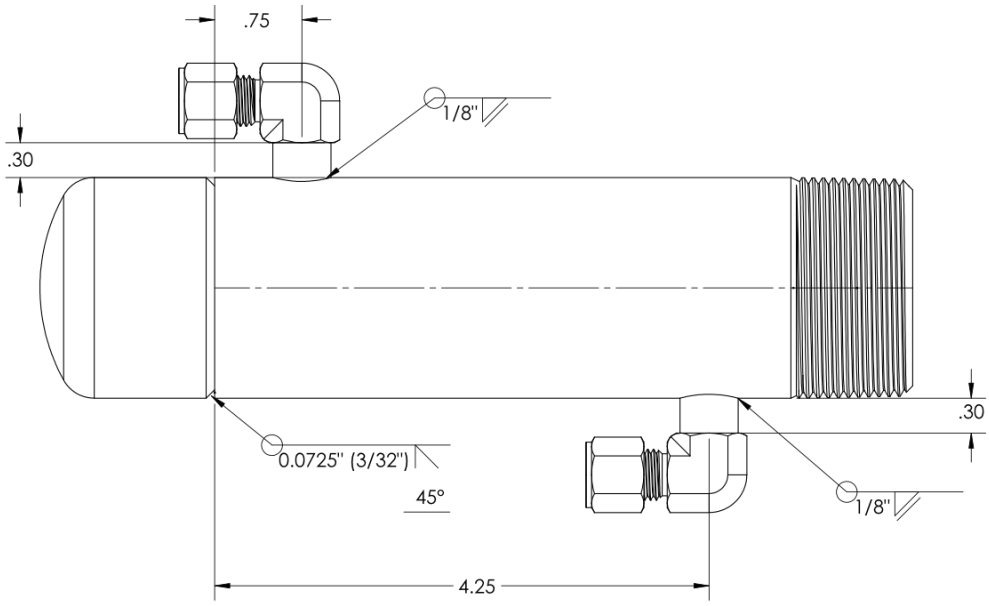

Figure 3.7: Engineering schematic of the main housing component designed by the author for use with dense tubular perovskite membranes. Note that all listed dimensions are in fractional customary units.

gas chromatograph (GC) to analyze experimental samples, and tubing to carry the gases between the different experimental apparatus components.

After leaving the gas storage bottle and passing through the regulator, each component gas entered an AALBORG GFC17 thermal mass flow controller. These controllers managed the volumetric flow rate of the gases by monitoring the temperature-dependent resistance gradient of temperature sensitive windings, which is linearly proportional to the instantaneous rate of flow. The GFC mass flow controllers used these measurements to control a proportionating electromagnetic valve and maintain the set gas flow rate [96]. The flow controllers had a maximum flow rate of 1000 mL/min (500 mL/min for carbon dioxide) and an accuracy of $\pm 1.0\%$ of the maximum flow rate [97].

Downstream of the flow controllers, the feed gas components were mixed and passed through a cutoff valve and a 2 µm filter before entering the membrane housing. Immediately

prior to entering the housing, a sampling valve allowed for testing of the feed gas composition. Similarly, the sweep gas passed through a cutoff valve and a 2 µm filter before entering the sweep side of the membrane housing. As on the feed side, a sampling valve, this time on the downstream side of the housing, allowed for testing of the combined permeate and sweep gas composition. System pressure was maintained separately for the feed and sweep sides of the apparatus using needle valves and pressure gauges immediately downstream of the membrane housing. Both pressure gauges were digital Omega Engineering Inc. model DPG1000B with an accuracy of ±0.25% and a range of 1 psig to 100 psig (7 kPa to 700 kPa) [98]. Additional pressure gauges were placed immediately downstream of the 2 µm filters on both the feed and sweep sides to allow for pressure monitoring upstream of the membrane housing. The thermocouple used to monitor the temperature of the system was an Omega Engineering Inc. K-Type thermocouple with an accuracy of either 2.2 °C or, if greater, ±0.75% [99]. Immediately upstream of the GC, a pressure gauge, 2 µm filter and controllable flow meter were placed to allow for additional monitoring and control of the permeate gas flow. Figure 3.8 below depicts the arrangement of the various apparatus components, while figure 3.9 shows the experimental facility as used.

In order to determine the membrane flux and selectivity, a gas chromatograph was used to measure the composition of both the feed and permeate gases. In this study, an Agilent 3000A Micro GC Gas Analyzer, depicted in figure 3.10, was used. This four-channel system can analyze fixed gases, light hydrocarbons, and volatile organic compounds. Each channel is entirely self-contained and can be set up to perform analysis on particular gases. During a test, the GC samples a "plug" of gas approximately 10 seconds in duration every three minutes. This means that transient or short time-scale effects cannot be reliably detected,

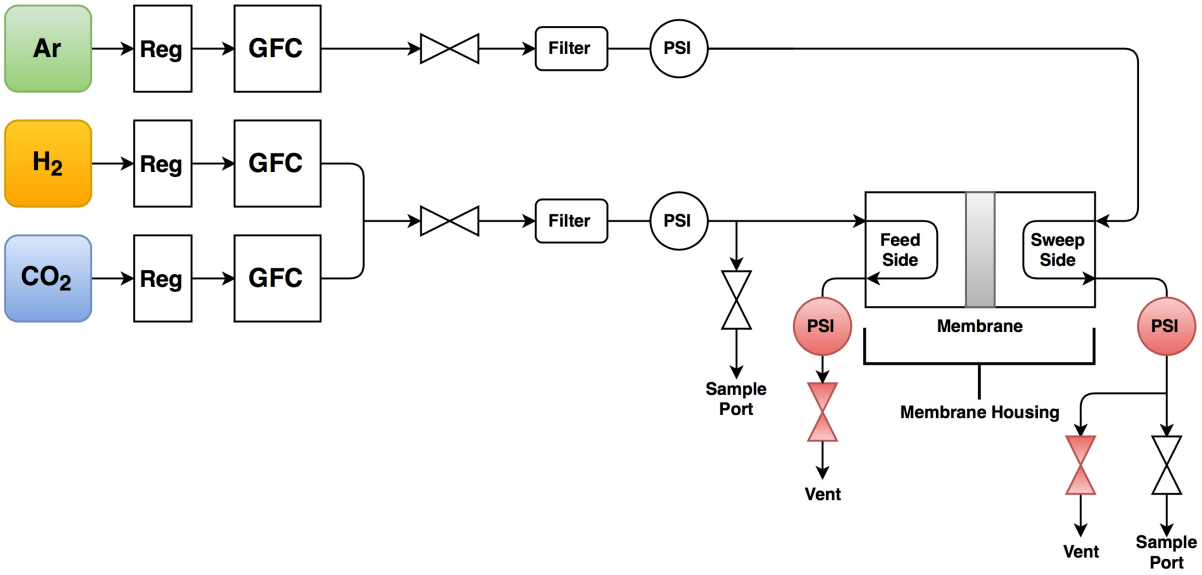

Figure 3.8: Diagram of the arrangement of experimental apparatus components used for testing of holey graphene membranes. The pressure gauges and valves highlighted in red are those used to monitor and control the pressure of the system.

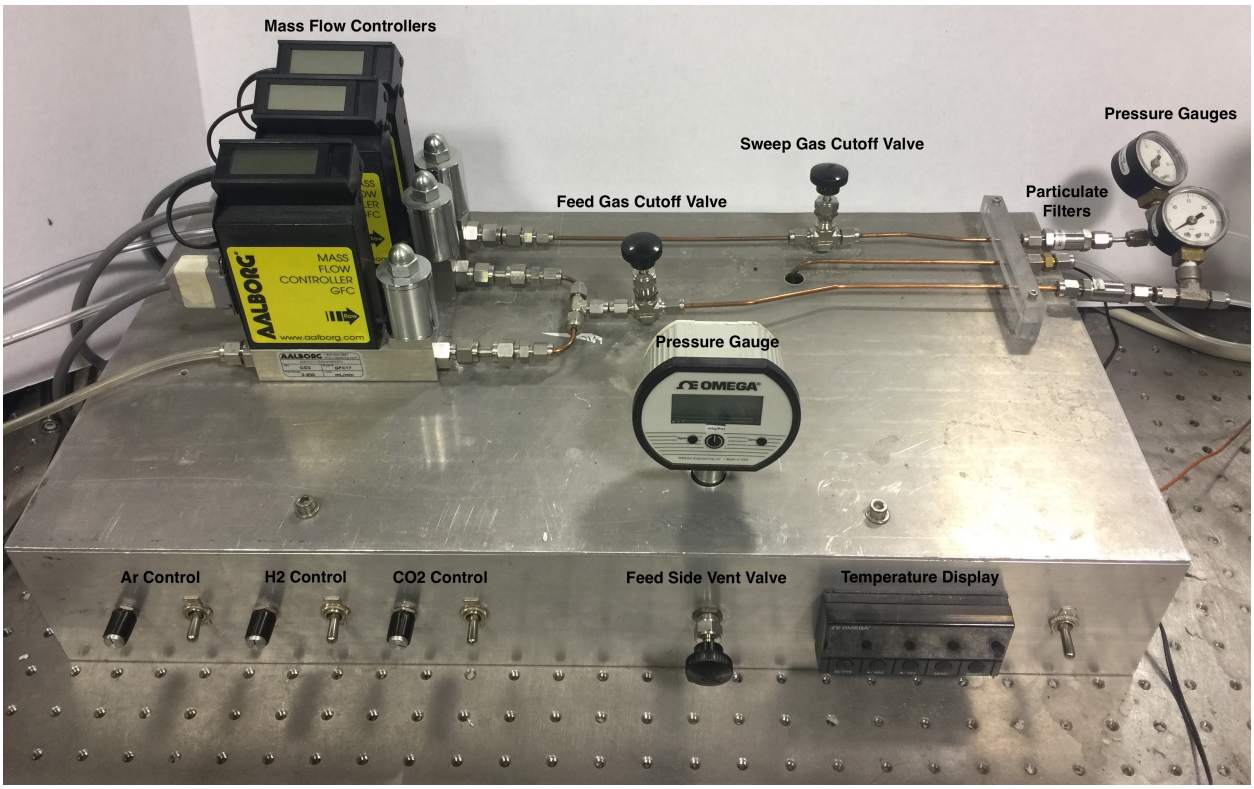

Figure 3.9: Picture of the gas flow control portion of the experimental facility used to test holey graphene hydrogen separation membranes. *Note:* the sample ports and components downstream of the sweep side of the membrane are not shown.

leaving steady-state analysis as the most effective use-case. Gas detection proceeds in three steps: injection, separation, and detection [100].

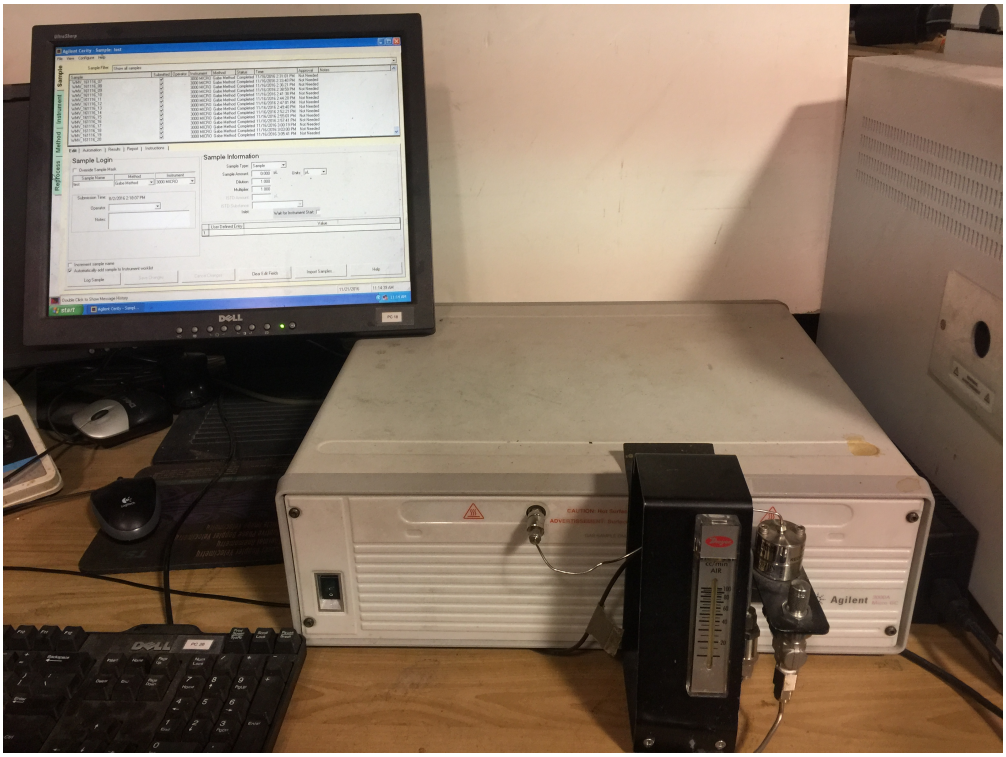

Figure 3.10: Agilent 3000A Micro GC Gas Analyzer used in this study.

During the injection phase, the gas sample was injected into the system through the heated inlet manifold, which ensured the sample was at the proper temperature and divided it into portions that were directed to the injector flow assemblies located within each detection channel. These assemblies included the injector chip, which opened and closed to allow the sample into the column for a specified time according to the detection program, as well as solenoid valves that used carrier gas to trigger the injector chip and the Electronic Pressure Control (EPC) valve that managed the column pressure. The samples were then drawn first into the injector sample loop and then into the detection column by a vacuum pump. Once on the detection column, the various components of the gas sample were separated

according to retentive or adsorptive interactions with the stationary phase material of the column. This difference in retention time allowed the GC channel to identify the component gases. Retention time can be based on molecular size, polarity, or boiling point according to stationary phase material choice. Once the sample components were separated, the gas entered the Thermal Conductivity Detector (TCD), in this case a Wheatstone bridge circuit. The TCD had two pathways in it: the reference path contained carrier gas only, while the analytical path included both carrier gas and sample gas. Differences in the thermal conductivity of the contents of the reference path and analytical path were measured by the TCD, which was then used to identify the unknown gas present in the analytical path [100]. It should be noted that the GC was unable to identify and measure either helium or argon, which were both used as carrier gases in the various sample columns. Because of this, argon was assumed to compose the entirety of the remainder of any gas samples whose mole percentage sum was less than 100%; e.g., if a GC sample indicated 35 mol% hydrogen and 25 mol% carbon dioxide, it was assumed that the remaining 40 mol% was comprised of pure argon.

3.3 Experimental Limitations

As with all experiments, limitations inherent in the design of the experimental equipment or procedure needed to be dealt with appropriately to ensure that the experimental results were valid. In this study, constraints regarding membrane construction, facility design, and feed gas purity were encountered.

3.3.1 Membrane Design Constraints

The first set of challenges that had to be addressed were related to the structure of the membranes themselves. Because the holey graphene films are created by simply compressing the into shape without any adhesive or underlying structural framework, the resulting films were much more brittle and fragile than the palladium-coated steel membranes previously used with this experimental apparatus. The specific modulus of holey graphene films was measured at roughly 693 MPa/(g/cm^3), somewhat less than that of high-density polyethylene [11,101]. Additionally, the holey graphene membranes ranged in thickness from 0.14 mm to 0.40 mm, compared to 1.5 mm for the palladium-based membranes. Due to these properties, significant modifications had to be made to the membrane mounting procedure to ensure the holey graphene membranes could be securely held in place without buckling, bowing or fracturing. Instead of simply compressing the membrane between the two halves of the membrane housing, a membrane holder was constructed of a copper washer and nitrile butadiene rubber (Buna-N) gaskets, depicted in figure 3.11. This holder sandwiched the membrane between a gasket on the upstream side and a copper washer on the downstream side, while also encircling it with an additional gasket. Together, these components acted to prevent feed gas leaks around the membrane, atmospheric leaks into the system, and reduce the force imparted onto the membrane by the pressure differential between the feed and sweep sides by rigidly supporting more of the downstream side of the membrane.

Use of this membrane holder influenced several important dimensions including the active area of the membrane, the membrane feed exposure volume and the surface area to volume ratio. These numbers had a significant impact on the performance of the

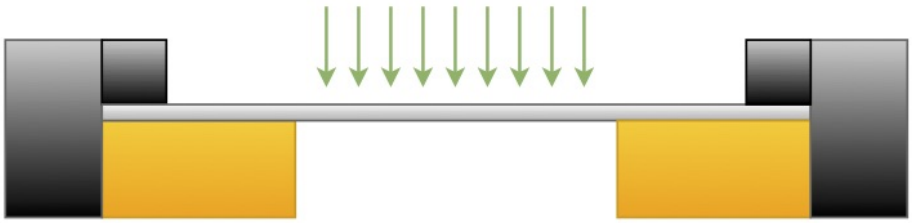

Figure 3.11: Cross-sectional schematic of the membrane holder constructed to securely mount the holey graphene membranes and form a gas-tight seal. Buna-N gaskets (black) provide a gas tight seal around the circumference of the membrane while the copper washer (orange) provides rigid support on the downstream side of the membrane.

membrane, so knowing their values and the impacts of changes to them was paramount to understanding the experimental results. Due to the presence of the copper washer directly downstream of the membrane, the effective area of the membrane was reduced to the area of the central opening in the washer. The washer used had an inner diameter of 5/8 in (1.59 cm), so the free area available for hydrogen permeation was roughly 199 mm^2. To find the membrane-feed exposure volume, three cylindrical volumes were calculated: the volume of the free space between the membrane face and the membrane-facing edge of the upstream copper washer, the volume of the internal hole of the upstream copper washer, and the volume of the membrane housing feed side cavity. Combining these volumes resulted in a total membrane-feed exposure volume of 1223 mm^3. Dividing this volume by the membrane active area revealed a surface area to volume ratio roughly half that of earlier experiments using this membrane housing. This change was due to the additional upstream volume introduced by the membrane holder. Because of this, the proportion of feed gas that passed directly over the surface of the membrane was reduced compared to earlier experiments. While this was detrimental to maximizing the hydrogen production potential

of the membrane; i.e., the proportion of hydrogen in the feed gas that permeated across the membrane, the consequences of this change in a proof-of-concept environment were negligible.

While use of the membrane holder significantly curtailed problems with membrane damage experienced in early testing, methods of further increasing the mechanical strength of the holey graphene membranes were also investigated. Some membrane samples were compressed between two films of Celgard 2325 battery separator material. This material was designed to act as a permeable membrane between the anode and cathode of batteries. These separators prevent short circuits within the battery structure while still permitting ions to pass from one side to the other to allow the circuit to be completed [102]. Many of the requisite properties for these separators (high porosity, consistent pore structure, chemical stability, and mechanical strength) made them ideal candidates for the purposes of this study. The specific membrane selected for use in this study, Celgard 2325, was a trilayer polypropylene-polyetheline-polypropylene membrane with a thickness of 25 µm, porosity of 39%, average pore diameter of 28 nm, puncture strength of 4.7 MPa using a blunt needle with an area of 0.785 mm^2, and yield strengths of 167 MPa (machine direction) and 14.7 MPa (transverse direction) [103–105]. Due to the high porosity and large pore size when compared to the holey graphene material, these films were able to act as a fully permeable support, not impeding the flow of gas across the membrane while lending fracture resistance and durability. Although direct burst pressure figures were not available for this material, a rough estimate of maximum pressure was calculated using generic properties for polypropylene and the following equation for the maximum pressure that a thin ductile membrane can withstand:

$$P_{max} = 6.4\frac{d_M \sigma_y^{3/2}}{2R_M\sqrt{E_M}}, \tag{3.1}$$

where $d_M = 25\,\mu m$ is the membrane thickness, $\sigma_y = 14.7\,MPa$ is the yield strength of the membrane, $R_M = 0.795\,cm$ is the membrane radius, and $E_M = 1300\,MPa$ is the Young's Modulus of the material [104, 106–108]. For this calculation, the lower transverse direction yield strength was used, along with a general Young's Modulus for polypropylene. Using these values, a maximum pressure of 15.6 kPa was calculated, only slightly higher than the planned experimental pressure differential of 13.8 kPa. Although each Celgard film would be a component in a membrane "system" including the holey graphene material and another film and would not need to withstand the entirety of the pressure differential individually, the low factor of safety for the films raised concerns about their ability to sufficiently bolster the membrane durability and strength. Due to this, freestanding films were pressure tested in the experimental apparatus at pressure differentials in excess of the experimental pressure, up to 40 kPa, without failure. No damage was observed to any Celgard-sandwiched membranes throughout the testing process at the test pressure differential of 13.8 kPa.

3.3.2 Facility Limitations

Although the vast majority of experimental limitations arose from the material being studied and were therefore incorporated into the previous section regarding membrane limitations, the experimental facility also presented issues that needed to be addressed. The biggest concern related to the experimental facility was control of the hydrogen partial pressure differential across the membrane. Because hydrogen diffusion across the membrane

was governed by this difference, it was vital to maximize this difference while keeping the total pressure differential below the level that would have resulted in damage to the membrane. Controlling the sweep gas flow rate had a significant impact on both the partial pressure differential and the measurability of the permeate gas samples. If the flow rate was too low, then the partial pressure difference would have been too low to induce significant hydrogen permeation. Conversely, if the flow rate was too high then the permeate could have been too diluted to be measured accurately by the GC. Relatedly, the experimental facility was located a significant distance away from the GC, necessitating approximately 8 m of 1/8 in (0.32 cm) flexible tubing to bridge the distance. This arrangement presented challenges in ensuring sufficient gas flow to the GC while maintaining a reasonable pressure downstream of the membrane. To satisfy all of these requirements, a sweep gas flow rate of 150 mL/min was used. Pressure and flow rate at the GC were controlled using the needle valve downstream of the membrane housing sweep side and the controllable flow meter attached to the GC, respectively. Use of a sweep gas in these experiments, however, simply replaced one problem (i.e., hydrogen being mixed with carbon dioxide) with another (hydrogen being mixed with the sweep gas). Due to this, sweep gas usage is generally limited to experimental, rather than commercial or industrial, applications. One notable exception is steam, because it is able to be condensed out of the product gas at a later stage. For these experiments, however, the advantages of using an inert sweep gas outweighed the potential drawbacks.

Another significant limitation of the experimental facility as used during these experiments was a product of the low operating temperatures of the Buna-N rubber gaskets (<100 °C), the flexible tubing (<200 °C), and the Celgard films (<165 °C) [103, 109, 110].

The melting points of these materials were significantly lower than the temperatures normally used for membrane-based hydrogen separation because of the danger of hydrogen embrittlement in traditional palladium- or ceramic-based membranes. In this study, however, the low operating temperatures were not a concern because the holey graphene membranes operated via molecular sieving and do not require the hydrogen molecules to dissociate. As such, these membranes were not susceptible to hydrogen embrittlement. This property was, in fact, one of the major advantages (along with their low cost) of holey graphene membranes when compared to other membrane separation technologies.

3.3.3 Feed Gas Impurities

Another significant concern regarding the validity of experimental results was related to the gases used during experimentation. The impacts of both the gases used and potential impurities within the feed and sweep gases were investigated to ensure they would not affect the experimental results. The gases used in this study were hydrogen, carbon dioxide, and argon. All three gases were sourced from Airgas, Inc. and were provided in industrial gas cylinders. Both the hydrogen and carbon dioxide were of "industrial" purity, with a stated purity of 100% [111, 112]. "High purity" argon was used, with a certified purity of 99.997% [113]. Testing was conducted with direct feeds of each gas to the GC to determine purity levels, with no trace components detected in any of the gases. As a result, all gases were treated as being completely pure during experimentation.

A final concern arose during initial measurements of gas samples by the GC. In all sample results, trace amounts of oxygen and nitrogen were recorded. While the presence of

carbon dioxide was expected in the permeate gas due to the expected selectivity values of the holey graphene membranes, this did not explain the presence of oxygen or nitrogen. An atmospheric leak into the system would explain the presence of both gases, but was not a satisfactory explanation due to two issues. Firstly, any atmospheric leak would result in a nitrogen to oxygen ratio of $3.76 : 1$, mirroring the ratio of the two gases in air. During testing, however, the ratio was measured at roughly $2.31 : 1$. Secondly, the entire experimental facility was pressurized to at least 20 kPa above atmospheric pressure to prevent leaks into the system and supply sufficient sampling pressure to the GC. During testing with the high-purity argon, although the aforementioned nitrogen and oxygen were detected, no carbon dioxide was detected, further indicating that this error was not due to an atmospheric leak. A review of earlier experimental results using this apparatus by Leyko revealed a similar error [6]. As suggested in that study, the GC was subjected to a bakeout routine as described in chapter 4. Additionally, the system's calibration was checked and confirmed to eliminate the possibility of erroneous measurements. The errors remained even after these steps were completed, however. A review of the equipment documentation revealed no accuracy figures for the machine aside from claims stating detection abilities in the low ppm range. Furthermore, the levels of these trace gases were found to be statistically the same across all experiments, lending further weight to the hypothesis that these were not readings of actual geed stream components. Because of this, the oxygen and nitrogen levels in the results were treated as a bias error of the GC equipment and ignored.

3.4 Uncertainty Analysis

Any measurement is, necessarily, only an approximation of the true value of the quantity of interest, or measurand. This can be due to equipment inaccuracies, measurement methodology, or other, unknown, variables. Because of this, a measurement is only valid when corrected to the maximum extent possible and accompanied by a statement of its associated uncertainty. Identification and correction of these errors, as well as the determination of their corresponding uncertainties, is therefore a vital part of obtaining valid experimental results [114].

3.4.1 Measurement Chain

The error associated with a given measurement can be broken down into two components: random and systematic. Random error arises from uncertain or stochastic variations in the conditions under which the measurement is taken. By their very nature, random errors cannot be compensated for, but they can be reduced to an expected value of zero through a sufficient number of repeated measurements. The potential influence of random errors on the measured value is incorporated into a measurement through the standard deviation of experimental results. It is important to note that this is an expression of the uncertainty associated with the measurement, rather than its error. In contrast to random error, systematic errors are due to recognized effects of "influence quantities," which are not the measurand but influence its result. These effects, when properly identified, can be compensated for by applying a correction to the measured value. Similar to how repeated measurements can reduce the expected value of the random error to zero, an

appropriate correction can reduce the expected value of the systematic error to zero. Just as the random error is subject to an uncertainty, however, so too is the correction of the systematic error, because the correction is determined from incomplete knowledge and is therefore itself subject to random error. Accordingly, a total of three adjustments must be made to a measured value in order to find the true value of the measurand: application of a correction for systematic errors, and incorporation of uncertainties due to random error associated with the measurement and the systematic error correction [114]. The relation between the measurement and the true value of the measurand is therefore:

$$M_{\text{true}} = M_{\text{meas}} + C_{\text{syst}} \pm \delta M_{\text{meas}} \pm \delta C_{\text{syst}}, \tag{3.2}$$

where M_{true} is the true value of the measurand, M_{meas} is the measured value (which includes both random and systemic error), C_{syst} is the correction for systematic error, δM_{meas} is the uncertainty associated with the random error influencing the measured value, and δC_{syst} is the uncertainty associated with the random error influencing the systematic error correction. In the context of this uncertainty analysis, systematic error (and its associated correction) was neglected and the analysis instead focused on the random error of the measurements δM_{meas}. Equation 3.2 was therefore simplified to equation 3.3

$$M_{\text{true}} = M_{\text{meas}} \pm \delta M_{\text{meas}}. \tag{3.3}$$

Table 3.2: Reported accuracy figures for experimental equipment.

Equipment	Model	Reported Accuracy
Mass Flow Controller	AALBORG GFC17	1.0% of max flow [97]
Pressure Gauge	Omega Engineering DPG1000B	±0.25% [98]
Thermocouple	Omega Engineering K-Type	2.2 °C [99]
Gas Chromatograph	Agilent 3000A Micro GC	Unknown (ppm) [100]

3.4.2 Sources of Uncertainty

The primary sources of uncertainty in this study were the mass flow controllers, pressure gauges, thermocouple, and GC. Uncertainty values for pressure and temperature measurements were not determined via the RSS method, but were instead assumed to be the previously mentioned reported accuracy figures for the various pieces of equipment, as listed in table 3.2.

Because the GC did not have a reported accuracy, the uncertainty associated with its results was calculated via the standard deviation of the set of measurements taken during each experiment. These standard deviation values were used to determine a 95% confidence interval for each measurement set, which was then assumed to be its uncertainty.

Determining the error introduced via leakage is an important consideration in analyses of the performance of dense membranes, such as those made from palladium. This is defined as that portion of the permeate gas that crosses the membrane through pores, cracks and scratches in the selective layer versus diffusing across the selective layer via dissociation. Understanding this error allowed for the calculation of the membranes' true performance

potential and facilitated more accurate comparisons between different membranes. In contrast, calculation of this error was both impossible and essentially meaningless for the holey graphene membranes used in this study. This was because all of the flux across the membrane was due to "leakage"—the hydrogen molecules did not dissociate and transport across the dense membrane lattice, but passed through pores in the material as intact molecules.

3.4.3 Determining Uncertainty Values

In order to accurately gauge the uncertainty associated with the experimental results, the root sum of squares (RSS) method was utilized:

$$\delta M_{\text{meas}} = \sqrt{\sum_{i=1}^{n} (\sigma_i^2)}, \tag{3.4}$$

where σ_i is the uncertainty associated with a specific error source i, generally expressed as the standard deviation of a set of measurements or the stated uncertainty of a piece of equipment. This method was used because there are several sources of potential error, each with unique levels of uncertainty. The RSS method produced a value most representative of the overall uncertainty associated with the experimental values.

Computing the overall error values for each experimental test was tedious and is therefore omitted here, but the results of these computations are included as error bars in the plots of experimental results shown in section 4.2.

Chapter 4: Experimental Results and Analysis

The work performed in this study relied heavily on the results of earlier work in the field of hydrogen separation, and particularly on research conducted by previous members of the University of Maryland Combustion Laboratory who created and modified the experimental facility used in this study. Because this experimental facility had been unused for some time, the first order of business was to ensure the system and its components were in good working order prior to experimentation.

Calibration was verified on the flow controllers, pressure gauges, thermocouple, and gas chromatograph. Additionally, the GC was subjected to a bakeout routine, in which the detection column temperatures were raised to between 160 °C and 180 °C and held for at least eight hours. This process clears any contaminants from the chromatography columns, preventing peak tailing and retention time shifts [100]. As mentioned in section 3.3.3, this process was repeated later in the study due to concerns regarding gas leakage. Once this process was completed, leak testing of the experimental facility commenced.

4.1 Leak Testing

After equipment calibration verification was completed, all of the facility's Swagelok fittings, valves, and tubing were inspected for overall condition and connection integrity.

Soapy water was applied to all connections to verify that the fittings had good seals, and tubing was pressurized and immersed in water to ensure no pinhole leaks were present. Several small leaks were identified and corrected in this process, resulting in a system that could maintain pressure and prevent intrusion of outside gases.

The membrane housing was then pressure tested to confirm gas tightness. For this test, the housing was pressurized to 50 psig (446 kPa) using argon at ambient temperature without a membrane installed. This ensured that both sides of the membrane housing were pressurized to the same level and prevented damage to the fragile membranes. Argon's non-reactivity as a noble gas made it an ideal candidate for use as the pressurizing gas, as it prevented any unintended adverse reactions from affecting the results of the pressure testing. Results of the pressure testing are shown in figure 4.1. These results were then compared to those observed by James and Leyko. Although there was a noticeable pressure loss over the course of the pressure test, the magnitude of the loss compared favorably to that seen by James and Leyko at ambient temperature [6, 7]. Achieving the improved performance seen by James and Leyko at elevated temperatures was not possible due to the concerns mentioned in section 3.3.2. Because the entire facility was pressurized above atmospheric pressure, and because of the slow rate of the leak, it was decided that the losses due to this leakage could be safely ignored in the analysis.

Once the integrity of the facility components was assured, attention was turned to confirming the gas tightness of the membrane mounting assembly. An impermeable polypropylene film was mounted in the assembly and the apparatus was pressurized to 5 psig (136 kPa) using hydrogen and carbon dioxide in a 1:1 molar ratio on the feed side and 3 psig (122 kPa) using argon on the sweep side, mirroring the conditions used in the permeation

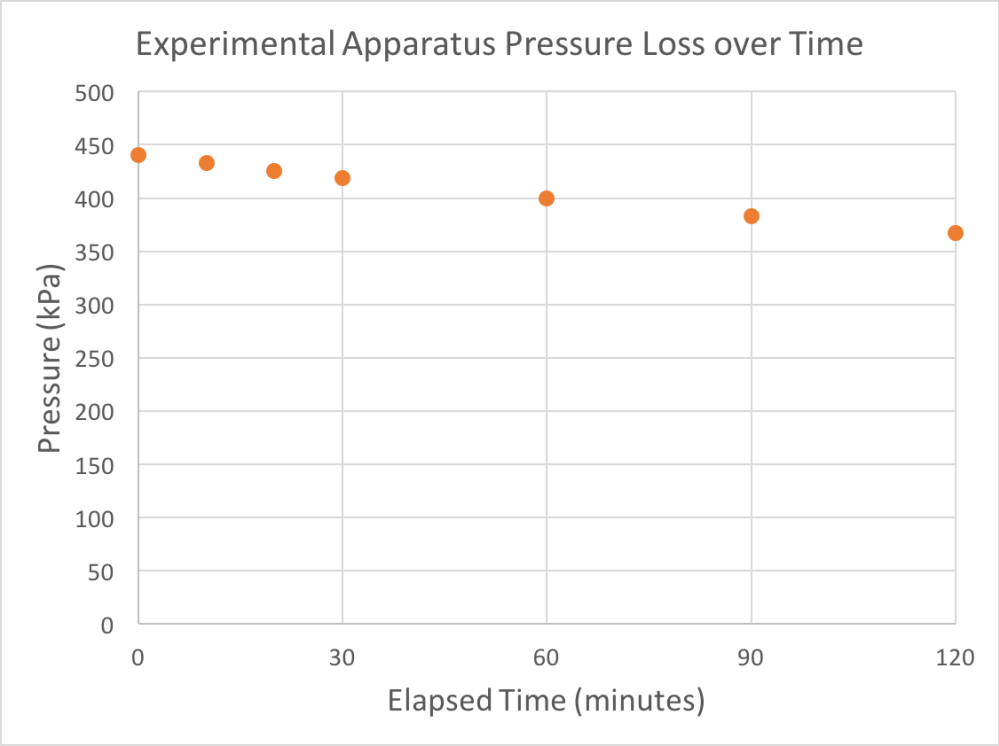

Figure 4.1: Experimental apparatus pressure test results. Test conducted at ambient temperature.

tests. Sampling of the permeate side revealed no hydrogen or carbon dioxide, confirming that the facility itself was gas tight between the two halves, with the only path from one side to the other being through the membrane. Pressure testing was not conducted with the holey graphene membranes in place due to concerns about the structural integrity of the membranes.

4.2 Permeation Experiments

After the pressure testing was completed, attention was turned towards conducting the hydrogen permeation tests. The ultimate goal of this study was to determine whether holey graphene membranes could be used to selectively separate hydrogen from a multicomponent feed gas stream designed to approximate biomass-derived syngas. A secondary goal was, if it

was determined that the holey graphene membranes could be used for hydrogen separation, to determine the effects of variations in the thickness and processing of these holey graphene membranes on their effectiveness in separating hydrogen from the feed gas stream. The data collected from these hydrogen separation experiments was used to calculate the flux values and selectivity of the tested membranes, which were then compared with the values attained through the use of other types of hydrogen separation membranes.

4.2.1 Hydrogen Permeation Experiments

Prior to conducting the separation tests themselves, initial work with the membranes and experimental apparatus led to the development of a standardized testing procedure that was used for all future experimentation. At the start of the test run, the GFCs were set to supply the appropriate gas flow rates to the apparatus with the downstream vent valves wide open on both the feed and permeate sides of the apparatus. Once the flow rates had stabilized, the feed-side and sweep-side pressures were carefully raised to the experimental pressure levels (136 kPa and 122 kPa, respectively) by throttling the vent valves, taking care to ensure the pressure differential across the membrane never exceeded 14 kPa. In some cases this pressure differential was not possible to attain due to the membrane integrity being compromised; in these cases the feed side pressure was held at 136 kPa and the sweep side was kept as low as possible. This was to reduce the risk of a membrane rupture due to excessive pressure differential. Once the experimental pressure differential was attained, the apparatus was monitored for approximately 10 minutes to ensure the system reached steady-state equilibrium before taking any measurements. It was expected that any permeation would

begin immediately upon the feed gas contacting the membrane surface and would remain relatively constant, but the decision was made to run the tests at steady state to prevent the influence of any unanticipated non-steady state factors and ensure consistency across experimental results.

Once the experimental setup had been running for the requisite ten minutes, the sampling tube was attached to the feed-side sample port and a series of tests were run to analyze the feed gas stream. The results of these tests were analyzed to ensure that the feed gas applied to the membrane of interest was in fact a 1:1 molar ratio of hydrogen and carbon dioxide. This both provided an accurate baseline for membrane selectivity calculations and eliminated the GFCs for hydrogen and carbon dioxide as an error source. By measuring the feed gas using the GC, the composition of the feed gas was able to be determined down to ppm accuracy.

After measurement of the feed gas stream was complete, the sampling tube was shifted to the sweep-side sample port and the vent valves were adjusted to bring the pressure differential back to the experimental pressure levels. The apparatus was again monitored for approximately 10 minutes to ensure steady-state equilibrium had been reached before sampling commenced. A series of twenty tests was then conducted, producing a dataset that consisted of measurements taken at three-minute intervals over the course of an hour. This provided both a robust dataset to minimize the uncertainty inherent in the results and a way to confirm that the membrane was indeed operating at steady state rather than experiencing flux and selectivity changes over time. All of the permeation experiments were conducted in an identical manner to ensure consistent parameters and make the experimental results as comparable as possible.

With these concerns fully addressed, the experimental testing proper could now begin. In all tests, a 1:1 molar ratio syngas analog composed of hydrogen and carbon dioxide was applied to the membrane at a rate of 500 ml/min. Simultaneously, a sweep stream of pure argon was maintained at a rate of 150 ml/min. These gas flow rates allowed for the attainment of the appropriate pressure levels on the feed and permeate sides of the membranes without requiring the vent valves to be completely closed. This was vital to ensure that the membrane was continually exposed to fresh feed gas with the requisite molar ratio. Additionally, these flow rates were sufficient to supply the GC with enough flow and pressure to produce accurate measurements. This flow profile was used with each membrane listed in table 3.1 and the performance of all the membranes was compared using the parameters of total flux, specific fluxes for hydrogen and carbon dioxide, and selectivity. Figure 4.2 shows the total flux values for each membrane. Figure 4.3 plots the total flux for the membranes subjected to the standard manufacturing process (membranes 1 through 3) as a function of their thickness.

As can be seen by comparing the data of membranes 1 through 3, the amount of holey graphene material used in the membranes' manufacture, and consequently the membranes' thickness, had an inverse relationship to the total flux through the membrane, a finding consistent with Richardson's Law (equation 2.14). The results showed that, over an increase in membrane thickness from roughly 0.14 mm to 0.28 mm, total flux through the membrane decreased by a factor of nearly 17. Similarly, sandwiching a membrane in between Celgard 2325 separator films or subjecting a membrane to a high-temperature reduction process also reduced their total flux. Compared to the standard 60 mg membrane, the results showed that the sandwiched membrane (membrane 4) exhibited roughly 85% less total flux and the

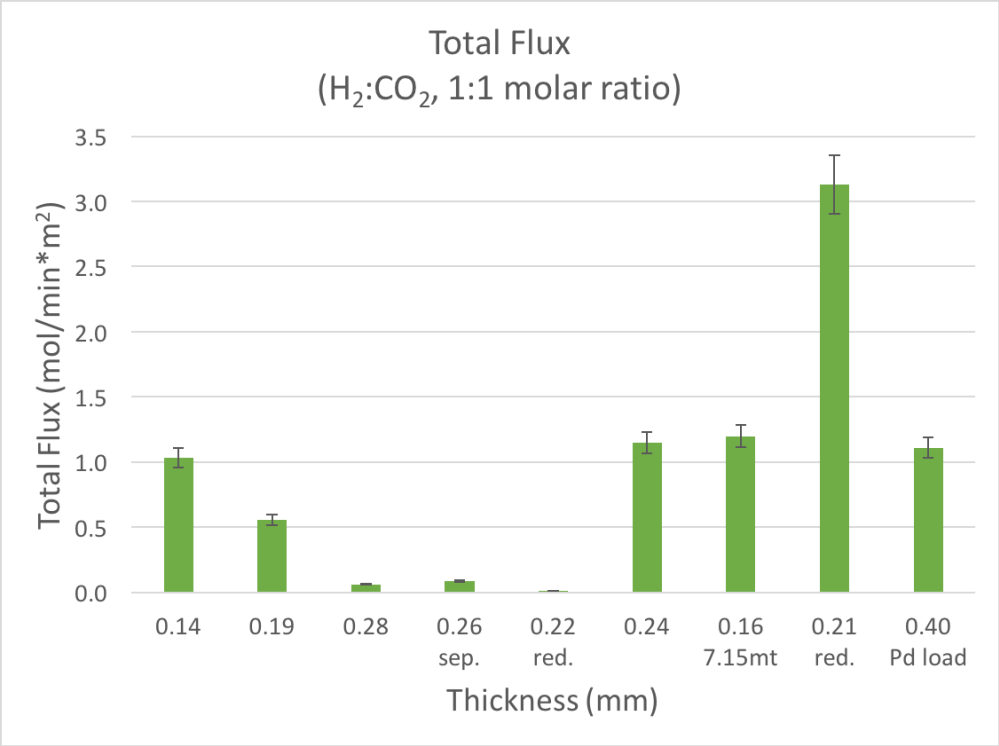

Figure 4.2: Total flux values for the holey graphene membranes investigated in this study. Refer to table 3.1 for membrane identification.

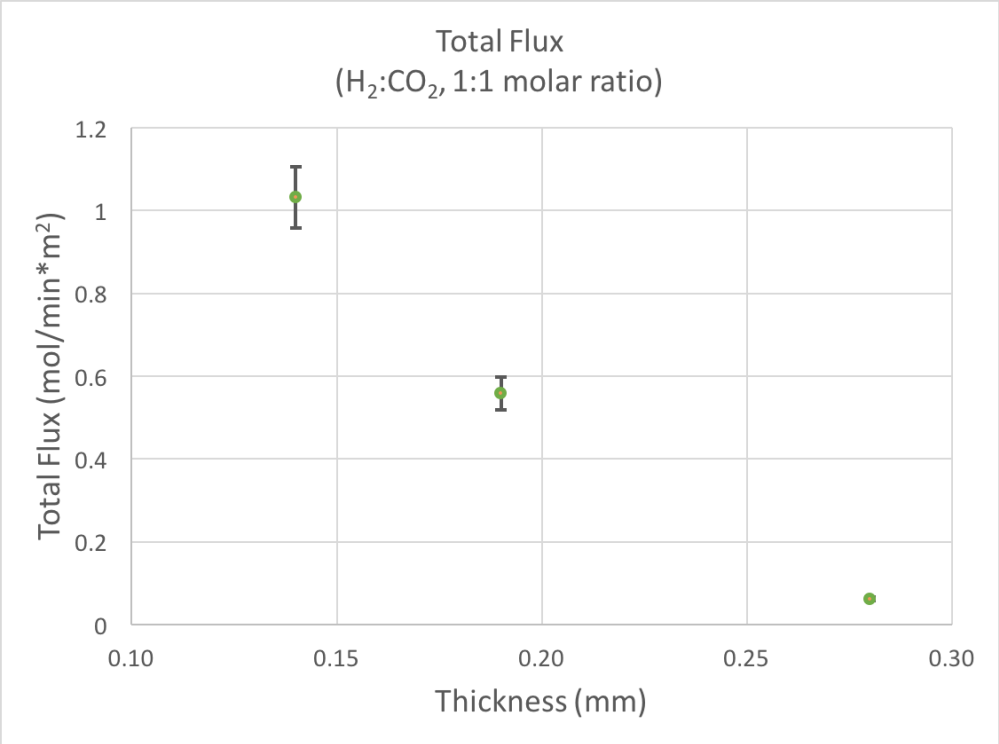

Figure 4.3: Total flux values plotted vs membrane thickness for holey graphene membranes subjected to the standard manufacturing process (membranes 1 through 3 in table 3.1).

reduced membrane (membrane 5) exhibited roughly 98% less total flux. Equally notable is the fact that several of the tested membranes (membranes 6 through 9) exhibited much higher total flux values than anticipated. The potential reasons for this excessive flux are discussed below in section 4.2.2. Although examining the total flux revealed the overall permeability of the various tested membranes, it did not provide insight into the effectiveness of the membranes in preferentially separating hydrogen from the feed gas. In order to examine this aspect of the membranes' performance, the flux of each gas species needed to be determined independently, and the selectivity for each membrane needed to be calculated. Figure 4.4 shows the flux of each species for the various membranes, while figure 4.6 shows the selectivity values for the membranes, as calculated using equation 2.22. Figures 4.5 and 4.7 plot the results for the membranes subjected to the standard manufacturing process (membranes 1 through 3) as a function of their thickness.

The most intriguing finding revealed by this data was that every membrane exhibited some level of preferential hydrogen permeation. The data for membranes 1 through 3 indicated a direct relationship between membrane thickness and selectivity. Additionally, an inverse relationship between total flux and membrane selectivity was also observed across all studied membranes. A very interesting result was the extremely high selectivity value for the reduced membrane (membrane 5). Unfortunately, this membrane also exhibited extremely low flux values, indicating limited usefulness outside of experimental applications. On the other end of the spectrum, the membranes identified in figure 4.2 as having excessive overall flux exhibited more-equal species flux and lower selectivity values. Additionally, the membrane manufactured using a higher compression pressure (membrane 7) did not exhibit improved performance, suggesting that after a certain point the holey graphene flakes cannot

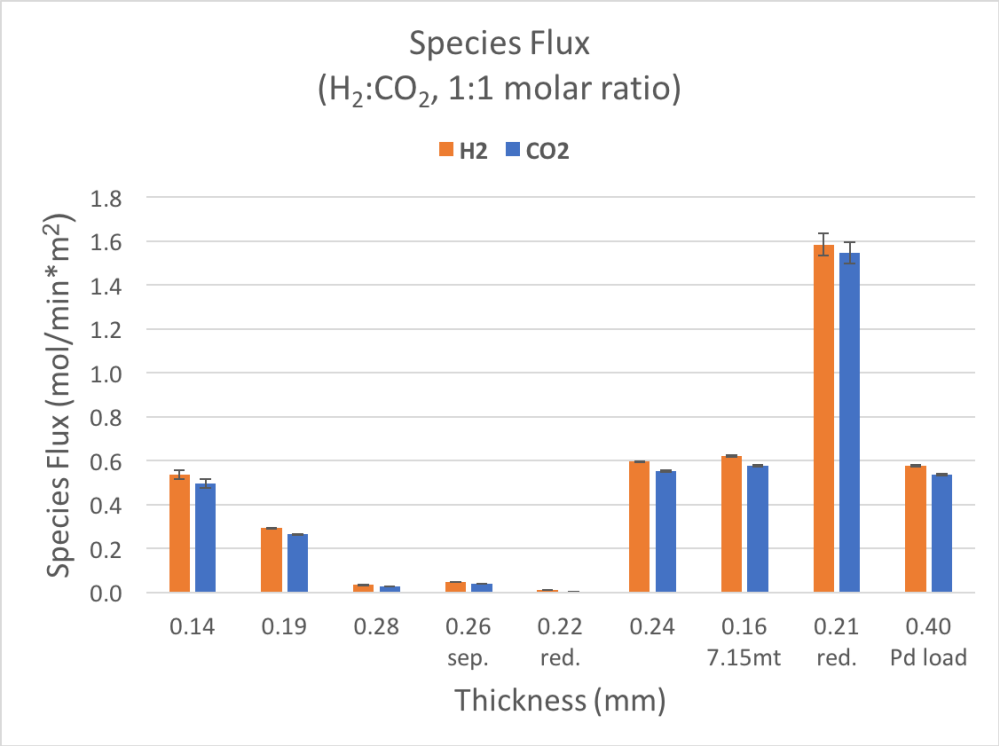

Figure 4.4: Hydrogen and carbon dioxide flux values for the holey graphene membranes investigated in this study. Refer to table 3.1 for membrane identification.

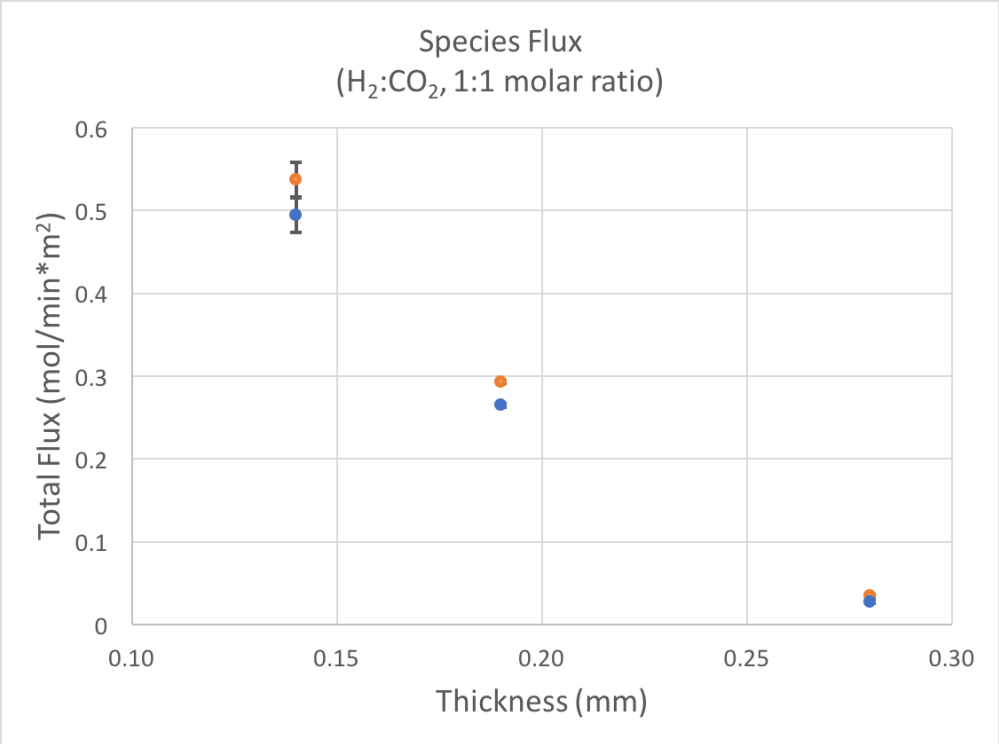

Figure 4.5: Species flux values plotted vs membrane thickness for holey graphene membranes subjected to the standard manufacturing process (membranes 1 through 3 in table 3.1).

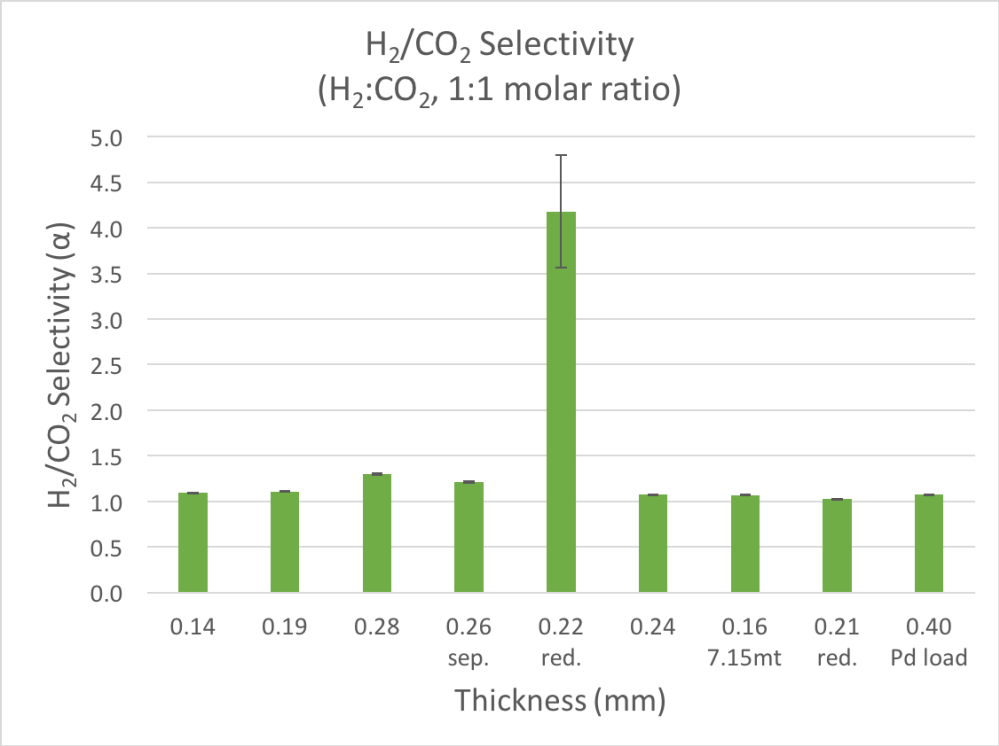

Figure 4.6: Hydrogen/Carbon Dioxide selectivity (α) values for the holey graphene membranes investigated in this study. Refer to table 3.1 for membrane identification.

be compressed more efficiently to increase selectivity. This once again pointed to a material degradation or failure as the culprit in these cases. Generally speaking, the best-performing membranes are those that intuitively make sense: thicker membranes, membranes combined with additional porous materials, and membranes subjected to a process designed to reduce the average pore size all exhibited lower overall flux and higher hydrogen selectivity than thinner membranes that were not subjected to additional processing steps.

4.2.2 Membrane Defects and Failures

An equally important finding of these experiments was the high rate of ineffective membranes produced. Four of the nine membranes tested (membranes 6 through 9) exhibited unsatisfactory performance as determined by excessive overall flux and low selectivity values.

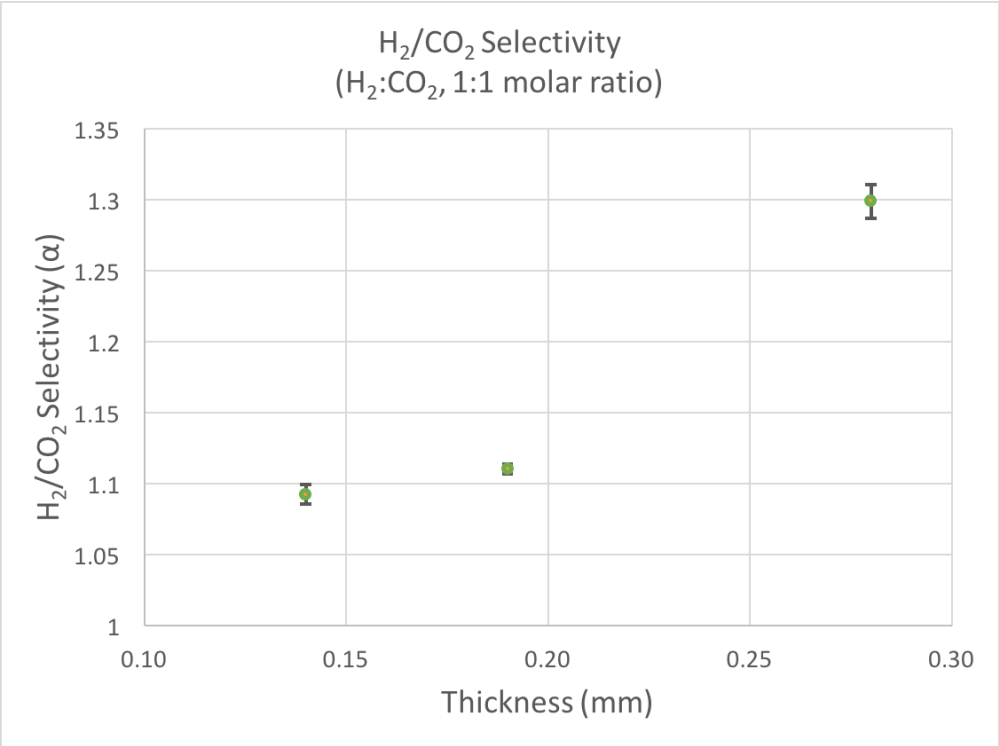

Figure 4.7: Hydrogen/Carbon Dioxide selectivity plotted vs membrane thickness for holey graphene membranes subjected to the standard manufacturing process (membranes 1 through 3 in table 3.1).

These four membranes were also unable to maintain the designed pressure differential during experimentation. This was a strong indicator that pinholes were present in the membrane, allowing unimpeded flow from the feed side to the permeate side. Although examining the membranes against a strong backlight revealed no pinholes prior to testing, further inspections after testing was completed identified pinholes in each of the four membranes discussed in this section. Two representative images of these pinholes are shown in figure 4.8. This pinhole formation was possibly a result of the manufacturing process; if the holey graphene material was unevenly distributed within the die, a thin area could be formed in the membrane which would not be subjected to the same compressive force as the rest of the membrane. This could result in a small section of the membrane that was not structurally sound and could therefore fail when exposed to the experimental pressure differential.

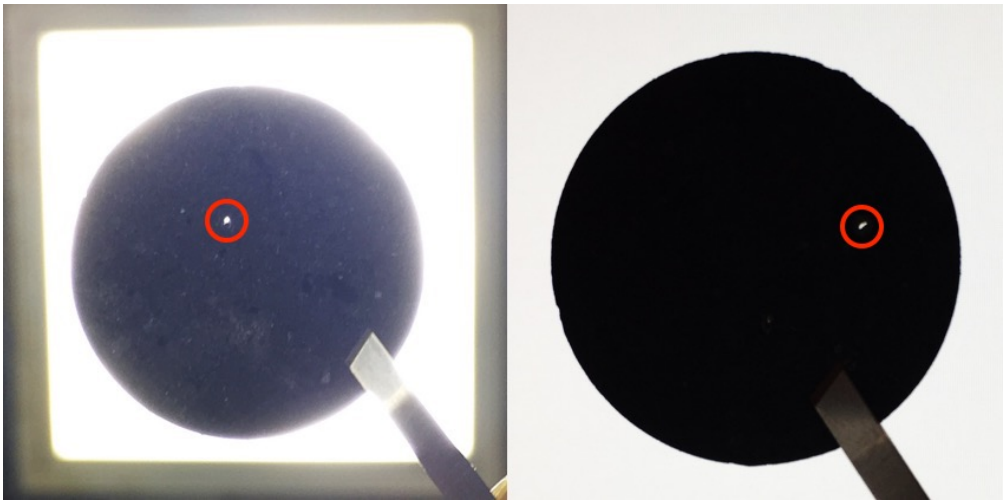

Figure 4.8: Pinholes observed in two holey graphene membranes after testing, circled in red. Neither of these membranes exhibited pinholes prior to experimentation. Note tweezers in the lower right-hand corner of each image, used to handle the membranes without damaging them.

A second, more catastrophic type of failure was observed in a smaller number of membranes, including a 60 mg membrane manufactured using a lower compression pressure and a second 75 mg membrane manufactured at the standard pressure. In these cases,

the center of the membrane suffered a blow out failure, resulting in a hole comprising approximately one-third of the membrane's surface area. One example of this failure is shown in figure 4.9. In both cases, the failures occurred while the experimental apparatus was being pressurized to experimental levels, indicating that these failures were a result of exceeding the maximum pressure differential for the membranes. Because the pressure differential never exceeded 14 kPa during the pressurization process, these membranes would have been unable to withstand the experimental conditions. Likely the lower manufacturing pressure used for the first membrane failed to compress it sufficiently to maintain structural integrity when exposed to the pressure differential, and the second membrane perhaps had a latent defect that produced a weak region which failed under pressure.

Figure 4.9: Blow out failure observed in a holey graphene membrane. Note the portion of material (right) that separated entirely from the membrane structure. Failure occurred during pressurization procedure before experimentation commenced.

Both of these failure mechanisms, as well as the rates at which they occurred, expose

considerable shortcomings in the holey graphene membranes as manufactured. Although these are significant challenges, the general operating principle was nevertheless validated for these membranes. Attention can now be turned to ways to improve both the membranes and the hydrogen separation process to increase the efficiency of the whole process.

4.2.3 Comparison to Existing Membrane Technologies

While this study's results were encouraging in and of themselves, their impact and implications needed context to be fully understood. Tables 4.1 and 4.2 compare the performance of the membranes investigated in this study with typical values for other hydrogen separation membrane types. It is apparent that the holey graphene membranes tested in this study do not compare very favorably with the established methods, particularly with regards to selectivity. The comparison in flux values is somewhat less useful, as the membranes were tested at a variety of pressure differentials, as noted in tables 4.1 and 4.2. Pressure-normalizing the results is not a perfect way to directly compare the performance of the membranes operating at significantly different pressure differentials, but the values produced still allow for general performance comparison and trend analysis.

The membranes examined in this study all exhibited preferential hydrogen diffusion, but also suffered from high failure rates. The performance of these membranes was successful in terms of a proof-of-concept using an untested material, but selectivity values in particular were unsatisfactory in the context of replacing existing hydrogen separation membranes.

Table 4.1: Flux comparison between the holey graphene membranes investigated in this study and several traditional hydrogen separation membrane materials.

Material	Pres. Diff. (kPa)	H_2 Flux (norm.) ($mol/min \cdot m^2 \cdot MPa$)
Holey Graphene (*This Study*)	14	0.7–38.6
Microporous Ceramic—General (Adhikari et al.) [5]	100	36–180
Dense Metallic (Pd)—General (Adhikari et al.) [5]	100	36–180
Pd on Al_2O_3 (CVD) (Basile et al.) [50]	30	3.3–6.7
Pd on Al_2O_3 (Electroless Plating) (Zhang) [9]	100	0.2
Pd (James) [7]	69	5.8
Pd (Leyko) [6]	69	34.8
Porous Carbon—General (Adhikari et al.) [5]	100	6–1200
Dense Perovskite Oxide (Yoon et al.) [40]	61	18
Dense Ceramic—General (Adhikari et al.) [5]	100	3.6–48

Table 4.2: Hydrogen/carbon dioxide selectivity comparison between holey graphene and several traditional hydrogen separation membrane materials.

Material	Pres. Diff. (kPa)	Selectivity H_2/CO_2 (α)
Holey Graphene (*This Study*)	14	1.1–4.2
Microporous Ceramic—General (Adhikari et al.) [5]	100	5–139
Dense Metallic (Pd)—General (Adhikari et al.) [5]	100	>1000
Pd on Al_2O_3 (CVD) (Basile et al.) [50]	30	5000
Pd on Al_2O_3 (Electroless Plating) (Zhang) [9]	100	700
Pd (Leyko) [6]	69	115
Porous Carbon—General (Adhikari et al.) [5]	100	4–20
CMS Film on Anodisc (Wang) [41]	100	3.5–4.2
Nanoporous Graphene (Liu) [115]	203	1.7
Dense Perovskite Oxide (Yoon et al.) [40]	61	Infinite[a]
Dense Ceramic—General (Adhikari et al.) [5]	100	>1000

[a] the operating mechanism for dense perovskite membranes (discussed in section 2.4.2) prevents any permeation of non-hydrogen molecules as long as the selective layer is intact.

Chapter 5: Conclusions and Recommendations for Future Work

In this study the ability of holey graphene membranes to preferentially separate hydrogen from a binary mixture of hydrogen and carbon dioxide was investigated. Additionally, the effects of certain manufacturing processes on the efficiency of these membranes were examined. Finally, the effectiveness of these membrane was compared to that of current hydrogen separation membranes.

5.1 Conclusions

During testing, membrane thickness was shown to have a significant effect on the overall flux rates, consistent with Richardson's Law. Moreover, the selectivity of the membranes was also found to increase as membrane thickness increased. Supplementary manufacturing steps, namely compressing the membrane material between two sheets of Celgard 2325 battery separator material, or subjecting the material to a high-temperature reduction process, also increased the membranes' selectivity. These increases in efficiency ranged widely in scope, with increases in thickness providing a modest bump in selectivity while the reduction process raised selectivity almost fourfold over the performance exhibited by the unreduced membrane of the same mass. As could be expected, these increases in hydrogen selectivity came with attendant decreases in overall membrane flux, with the reduced holey graphene membrane

exhibiting significantly lower overall flux than the unreduced membranes.

Another important finding determined by this study was the relative fragility of these membranes, as well as the difficulties encountered in reliably manufacturing them. Pinhole formation and pressure differential resiliency were both concerns that arose during this study, with multiple membranes failing via each of these mechanisms.

The third major finding of this study was related to the dense doped perovskite membranes investigated for their suitability in hydrogen separation processing. Although no tests were conducted using these membranes, it was determined that these membranes would be well-suited to hydrogen separation. Several of their material properties, including their extremely high selectivity, high flux potential, high temperature resistance, and relatively low cost, mean this style of membrane presents several unique advantages for separating hydrogen from biomass-derived syngas.

5.2 Contributions

This study showed that membranes produced by mechanically compressing holey graphene material can be used to preferentially separate hydrogen from a 1:1 molar ratio feed gas composed of hydrogen and carbon dioxide. Certain changes to the processing of these membranes was shown to increase their efficiency at allowing hydrogen to preferentially diffuse across their thickness, especially by subjecting the membrane to a high-temperature reduction process. This increase in hydrogen/carbon dioxide selectivity comes at the cost of decreased flux across the membrane, which presents implications for overall membrane suitability. These results raise the possibility of a new class of hydrogen separation

membrane, able to be manufactured more economically and immune to the ravages of hydrogen embrittlement.

This study also showed that dense perovskite membranes offer an attractive potential solution for extracting hydrogen from biomas-derived syngas. The material characteristics determined during this study indicate that this style of membrane would perform well under the conditions at which post-gasification hydrogen separation is performed. This information opens the door for using a heavily-researched and highly effective membrane type in a novel use case to advance the state of the carbon-neutral hydrogen energy economy.

5.3 Recommendations for Future Work

Throughout the course of this study, several avenues for future investigations presented themselves. Due to their being outside of the scope of this project, they have been listed here as recommendations for future work. These areas of investigation include further characterization work on the holey graphene membrane and potential improvements to the manufacturing process.

5.3.1 Future Characterization Work

All of the tests in this study occurred at ambient temperature due to concerns about the melting point of the Buna-N o-rings and Celgard films used during the experiments. Use of materials more resistant to high temperatures would allow for the study of the effects of temperature on the permeability of the holey graphene membranes, up to a limit of roughly 350 °C due to concerns about further oxidation of the material.

Adjustments to the gases used in the experiments is another area ripe for investigation. Tests using nitrogen, carbon monoxide or methane in the feed stream would provide further information related to the efficacy of holey graphene as a hydrogen separation membrane for biomass-derived syngas. Investigation of the behavior of the membranes when exposed to multi-component feed gases would provide insights into their utility in use cases outside of the laboratory. In addition to changing the feed gas composition, use of steam as the sweep gas would provide important data regarding the commercial and industrial viability of holey graphene membranes, as steam is easily condensed out of the permeate gas downstream of the separation process.

Although there were no indications of changes in membrane behavior over time during this study, subjecting the membranes to experimental conditions for extended periods of time (multiple hours or even days) would provide further data regarding the material's ability to serve as a hydrogen separation membrane in industrial applications and ensure there weren't any slow-acting non-steady state components to the membranes' behavior.

Because the holey graphene membranes generally exhibited higher overall flux and lower selectivity values compared to traditional hydrogen separation membranes, one intriguing avenue of future work would be the use of several membranes aligned in series. Since the holey graphene material is inexpensive, relatively speaking, it could be feasible to use a large bank of successive membranes to incrementally filter the feed gas into highly pure hydrogen gas. Because the thinnest membrane (the 44.7 mg membrane) exhibited the highest overall flux while also showing preferential diffusion, further study of this membrane, especially in a bank of membranes, is potentially the most promising avenue of study.

Finally, doped perovskite membranes present an interesting research opportunity in

the field of hydrogen separation. Further characterization and experimental testing of these membranes is highly recommended due to their potential for extremely high selectivity values for hydrogen and all other syngas components, potential for high flux values, and ability to incorporate WGS and CDRM equilibrium point shifting into the hydrogen separation process.

5.3.2 Manufacturing Process Improvements

The flip side of potential future work is improvements related to the holey graphene membranes themselves. During this study great care needed to be taken to prevent the membranes from fracturing or shattering, and several membranes were compromised by pinholes that prevented them from acting as effective selective membranes. If the membranes could be adhered to a more rigid porous surface, such as the porous metal substrates commonly used to support thin palladium membranes, the increase in structural rigidity could allow for a higher pressure differential or increased flow rates, resulting in a more effective membrane. In the same vein, developing a method by which pressure could be applied to the membrane material more evenly during the manufacturing process would minimize the risk of pinhole formation and produce more durable, resilient membranes.

Bibliography

[1] A. Haryanto, S. Fernando, N. Murali, and S. Adhikari, "Current status of hydrogen production techniques by steam reforming of ethanol: A review," *Energy & Fuels*, vol. 19, no. 5, pp. 2098–2106, 2005.

[2] J. R. Bartels, M. B. Pate, and N. K. Olson, "An economic survey of hydrogen production from conventional and alternative energy sources," *International Journal of Hydrogen Energy*, vol. 35, no. 16, pp. 8371–8384, 2010.

[3] M. Asadullah, S.-i. Ito, K. Kunimori, M. Yamada, and K. Tomishige, "Energy efficient production of hydrogen and syngas from biomass: development of low-temperature catalytic process for cellulose gasification," *Environmental Science & Technology*, vol. 36, no. 20, pp. 4476–4481, 2002. PMID: 12387426.

[4] J. W. Phair and R. Donelson, "Developments and design of novel (non-palladium-based) metal membranes for hydrogen separation," *Industrial & Engineering Chemistry Research*, vol. 45, no. 16, pp. 5657–5674, 2006.

[5] S. Adhikari and S. Fernando, "Hydrogen membrane separation techniques," *Industrial & Engineering Chemistry Research*, vol. 45, no. 3, pp. 875–881, 2006.

[6] A. B. Leyko, "Effect of composition on hydrogen permeation through palladium based membranes," Master's thesis, University of Maryland, College Park, 2013.

[7] R. T. James, "Temperature and pressure effects on hydrogen permeation in palladium based membranes," Master's thesis, University of Maryland, College Park, 2010.

[8] K. Atsonios, K. D. Panopoulos, A. Doukelis, A. K. Koumanakos, E. Kakaras, T. A. Peters, and Y. C. van Delft, *Introduction to palladium membrane technology*, ch. 1, pp. 1–22. No. 68 in Woodhead Publishing Series in Energy, Cambridge, UK: Woodhead Publishing-Elsevier, 1st ed., 2015.

[9] K. Zhang, H. Gao, Z. Rui, Y. Lin, and Y. Li, "Preparation of thin palladium composite membranes and application to hydrogen/nitrogen separation," *Chinese Journal of Chemical Engineering*, vol. 15, no. 5, pp. 643–647, 2007.

[10] Z. Tao, L. Yan, J. Qiao, B. Wang, L. Zhang, and J. Zhang, "A review of advanced proton-conducting materials for hydrogen separation," *Progress in Materials Science*, vol. 74, pp. 1–50, 2015.

[11] X. Han, M. R. Funk, F. Shen, Y.-C. Chen, Y. Li, C. J. Campbell, J. Dai, X. Yang, J.-W. Kim, Y. Liao, C. W., V. Barone, Z. Chen, Y. Lin, and L. Hu, "Scalable holey graphene synthesis and dense electrode fabrication toward high-performance ultracapacitors," *ACS Nano*, vol. 8, no. 8, pp. 8255–8265, 2014.

[12] S. Dunn, "Hydrogen futures: Toward a sustainable energy system," *International Journal of Hydrogen Energy*, vol. 27, no. 3, pp. 235–264, 2002.

[13] G. J. Grashoff, C. E. Pilkington, and C. W. Corti, "The purification of hydrogen: A review of the technology emphasizing the current status of palladium membrane diffusion," *Platinum Metals Review*, vol. 27, no. 4, pp. 157–169, 1983.

[14] C. Higman and M. van der Burgt, *Gasification*. Burlington, MA: Gulf Professional Publishing-Elsevier, 2nd ed., 2008.

[15] A. V. Bridgwater and S. A. Bridge, *A Review of Biomass Pyrolysis and Pyrolysis Technologies*, ch. 2, pp. 11–92. New York, NY: Elsevier Science, 1st ed., 1991.

[16] I. A. Gomaa, *High Temperature Steam Gasification of Solid Wastes: Characteristics and Kinetics*. PhD thesis, University of Maryland, 2011.

[17] H. Yang, R. Yan, H. Chen, D. H. Lee, and C. Zheng, "Characteristics of hemicellulose, cellulose and lignin pyrolysis," *Fuel*, vol. 86, no. 12–13, pp. 1781–1788, 2007.

[18] P. Joseph, S. Tretsiakova-McNally, and S. McKenna, "Characterization of cellulosic wastes and gasification products from chicken farms," *Waste Management*, vol. 32, no. 4, pp. 701–709, 2012. Solid Waste Gasification.

[19] M. S. Hussein, K. G. Burra, R. S. Amano, and A. K. Gupta, "Effect of oxygen addition in steam gasification of chicken manure," *Fuel*, vol. 189, pp. 428–435, 2017.

[20] W. Wang, X. Pan, X. Zhang, W. Yang, and G. Xiong, "The effect of co-existing nitrogen on hydrogen permeation through thin Pd composite membranes," *Separation and Purification Technology*, vol. 54, no. 2, pp. 262–271, 2007.

[21] F. Gallucci, F. Chiaravalloti, S. Tosti, E. Drioli, and A. Basile, "The effect of mixture gas on hydrogen permeation through a palladium membrane: Experimental study and theoretical approach," *International Journal of Hydrogen Energy*, vol. 32, no. 12, pp. 1837–1845, 2007.

[22] F. Guazzone, E. E. Engwall, and Y. H. Ma, "Effects of surface activity, defects and mass transfer on hydrogen permeance and n-value in composite palladium-porous stainless steel membranes," *Catalysis Today*, vol. 118, no. 1–2, pp. 24–31, 2006. Proceedings of the 7th International Conference on Catalysis in Membrane Reactors.

[23] H. É. S. Deville and L. J. Troost, "Comptes rendus," no. 57, p. 965, 1863.

[24] H. É. S. Deville, "Comptes rendus," no. 59, p. 102, 1864.

[25] T. Graham, "On the absorption and dialytic separation of gases by colloid septa," *Philosophical Transactions of the Royal Society of London*, vol. 156, pp. 399–439, January 1866.

[26] B. D. Morreale, M. V. Ciocco, R. M. Enick, B. I. Morsi, B. H. Howard, A. V. Cugini, and K. S. Rothenberger, "The permeability of hydrogen in bulk palladium at elevated temperatures and pressures," *Journal of Membrane Science*, vol. 212, no. 1–2, pp. 87–97, 2003.

[27] W. O. Snelling, "Apparatus for separating gases." Patent, March 1916. US Patent 1,174,631.

[28] A. G. Knapton, "Palladium alloys for hydrogen diffusion membranes: A review of high permeability materials," *Platinum Metals Review*, vol. 21, pp. 44–50, April 1977.

[29] J. B. Hunter, "Silver-palladium film for separation and purification of hydrogen." Patent, December 1956. US Patent 2,773,561.

[30] H. Connor, "Palladium alloy diffusion cells: Commercial units for the production of ultra-pure hydrogen," *Platinum Metals Review*, vol. 6, no. 4, pp. 130–135, 1962.

[31] A. K. Prabhu and S. T. Oyama, "Highly hydrogen selective ceramic membranes: application to the transformation of greenhouse gases," *Journal of Membrane Science*, vol. 176, no. 2, pp. 233–248, 2000.

[32] M. W. Lee, "Separation membrane development for hydrogen," tech. rep., U. S. Department of Energy, August 2000.

[33] D. Lee and S. T. Oyama, "Gas permeation characteristics of a hydrogen selective supported silica membrane," *Journal of Membrane Science*, vol. 210, no. 2, pp. 291–306, 2002.

[34] S.-J. Song, E. D. Wachsman, J. Rhodes, S. E. Dorris, and U. Balachandran, "Hydrogen permeability of $SrCe_{1-x}M_xO_{3-\delta}(x = 0.05, M = Eu, Sm)$," *Solid State Ionics*, vol. 167, no. 1–2, pp. 99–105, 2004.

[35] H. Yoon, S. Song, T. Oh, J. Li, K. L. Duncan, and E. D. Wachsman, "Fabrication of thin-film $SrCe_{0.9}Eu_{0.1}O_{3-\delta}$ hydrogen separation membranes on $Ni-SrCeO_3$ porous tubular supports," *Journal of the American Ceramic Society*, vol. 92, pp. 1849–1852, August 2009.

[36] J. Li, H. Yoon, T.-K. Oh, and E. D. Wachsman, "High temperature $SrCe_{0.9}Eu_{0.1}O_{3-\delta}$ proton conducting membrane reactor for H_2 production using the water–gas shift reaction," *Applied Catalysis B: Environmental*, vol. 92, no. 3–4, pp. 234–239, 2009.

[37] T.-K. Oh, H. Yoon, and E. D. Wachsman, "Effect of Eu dopant concentration in $SrCe_{1-x}Eu_xO_{3-\delta}$ on ambipolar conductivity," *Solid State Ionics*, vol. 180, no. 23–25, pp. 1233–1239, 2009.

[38] T. Oh, H. Yoon, J. Li, and E. D. Wachsman, "Hydrogen permeation through thin supported $SrZr_{0.2}Ce_{0.8-x}Eu_xO_{3-\delta}$ membranes," *Journal of Membrane Science*, vol. 345, no. 1–2, pp. 1–4, 2009.

[39] T. Oh, J. Li, H. Yoon, and E. D. Wachsman, "Stability of $SrCe_{0.9}Eu_{0.1}O_{3-\delta}$ and $SrZr_{0.2}Ce_{0.7}Eu_{0.1}O_{3-\delta}$ under H_2 atmospheres," *Ionics*, vol. 15, no. 5, pp. 525–530, 2009.

[40] H. Yoon, T. Oh, J. Li, K. L. Duncan, and E. D. Wachsman, "Permeation through $SrCe_{0.9}Eu_{0.1}O_{3-\delta}$/Ni−$SrCeO_3$ tubular hydrogen separation membranes," *Journal of The Electrochemical Society*, vol. 156, no. 7, pp. B791–B794, 2009.

[41] L.-J. Wang and F. C.-N. Hong, "Effects of surface treatments and annealing on carbon-based molecular sieve membranes for gas separation," *Applied Surface Science*, vol. 240, no. 1–4, pp. 161–174, 2005.

[42] L.-J. Wang and F. C.-N. Hong, "Carbon-based molecular sieve membranes for gas separation by inductively-coupled-plasma chemical vapor deposition," *Microporous and Mesoporous Materials*, vol. 77, no. 2–3, pp. 167–174, 2005.

[43] H. Kita, K. Nanbu, H. Maeda, and K. Okamoto, *Gas Separation and Pervaporation through Microporous Carbon Membranes Derived from Phenolic Resin*, vol. 876 of *ACS Symposium Series*, ch. 14, pp. 203–217. Washington, D.C.: American Chemical Society, 1st ed., 2004.

[44] G. E. Keller, *Gas-Adsorption Processes: State of the Art*, vol. 223 of *ACS Symposium Series*, ch. 8, pp. 145–169. Washington, D.C.: American Chemical Society, 1st ed., 1983.

[45] T. Keller and G. Shahani, "PSA technology: Beyond hydrogen purification," *Chemical Engineering*, January 2016.

[46] P. Cen and R. T. Yang, "Bulk gas separation by pressure swing adsorption," *Industrial & Engineering Chemistry Fundamentals*, vol. 25, no. 4, pp. 758–767, 1986.

[47] J. A. Delgado, V. I. Agueda, M. A. Uguina, J. L. Sotelo, and P. Brea, "Hydrogen recovery from off-gases with nitrogen-rich impurity by pressure swing adsorption using CaX and 5A zeolites," *Adsorption*, vol. 21, no. 1, pp. 107–123, 2015.

[48] J. Xiao, Y. Peng, P. Bénard, and R. Chahine, "Thermal effects on breakthrough curves of pressure swing adsorption for hydrogen purification," *International Journal of Hydrogen Energy*, vol. 41, no. 19, pp. 8236–8245, 2016. Special Issue on Progress in Hydrogen Production and Applications (ICH2P-2015), 3–6 May 2015, Oshawa, Ontario, Canada.

[49] B. Li, G. He, X. Jiang, Y. Dai, and X. Ruan, "Pressure swing adsorption/membrane hybrid processes for hydrogen purification with a high recovery," *Frontiers of Chemical Science and Engineering*, vol. 10, no. 2, pp. 255–264, 2016.

[50] M. De Falco, L. Marrelli, and G. Iaquaniello, *Membrane Reactors for Hydrogen Production Processes*. London, UK: Springer, 1st ed., 2011.

[51] A. Unemoto, A. Kaimai, K. Sato, T. Otake, K. Yashiro, J. Mizusaki, T. Kawada, T. Tsuneki, Y. Shirasaki, and I. Yasuda, "Surface reaction of hydrogen on a palladium alloy membrane under co-existence of H_2O, CO, CO_2 or CH_4," *International Journal of Hydrogen Energy*, vol. 32, no. 16, pp. 4023–4029, 2007. TMS06: Symposium on Materials in Clean Power Systems.

[52] L. Li, *Nanoporous Polymers for Membrane Applications*. PhD thesis, Technical University of Denmark, The Danish Polymer Centre, Department of Chemical and Biochemical Engineering, Technical University of Denmark, Sølvtofts Plads, DK-2800 Kgs. Lyngby, Denmark, April 2012.

[53] W. He, W. Lv, and J. H. Dickerson, *Gas Diffusion Mechanisms and Models*, ch. 2, pp. 9–17. Springer Briefs in Energy, Cham, SUI: Springer International Publishing, 1st ed., September 2014.

[54] T.-K. Oh, *Determination of Optimal Europium Dopant Concentration in Strontium Cerate Mixed-Conducting Ceramic Membrane for Maximum Hydrogen Production*. PhD thesis, University of Florida, 2008.

[55] S. Stotz and C. Wagner, "Die löslichkeit von wasserdampf und wasserstoff in festen oxiden," *Berichte der Bunsengesellschaft für Physikalische Chemie*, vol. 70, no. 8, pp. 781–788, 1966.

[56] M. Mulder, *Basic Principles of Membrane Technology*. Dordrecht, NED: Kluwer Academic, 2nd ed., 1996.

[57] J. M. Polfus, W. Xing, M.-L. Fontaine, C. Denonville, P. P. Henriksen, and R. Bredesen, "Hydrogen separation membranes based on dense ceramic composites in the $La_{27}W_5O_{55.5}$−$LaCrO_3$ system," *Journal of Membrane Science*, vol. 479, pp. 39–45, 2015.

[58] D. L. McKinley, "Method for hydrogen separation and purification." Patent, April 1966. US Patent 3,247,648.

[59] Y. Lin, K. A. Watson, J.-W. Kim, D. W. Baggett, D. C. Working, and J. W. Connell, "Bulk preparation of holey graphene via controlled catalytic oxidation," *Nanoscale*, vol. 5, pp. 7814–7824, 2013.

[60] M. J. Allen, V. C. Tung, and R. B. Kaner, "Honeycomb carbon: A review of graphene," *Chemical Reviews*, vol. 110, no. 1, pp. 132–145, 2010.

[61] K. S. Novoselov, A. K. Geim, S. V. Morozov, D. Jiang, Y. Zhang, S. V. Dubonos, I. V. Grigorieva, and A. A. Firsov, "Electric field effect in atomically thin carbon films," *Science*, vol. 306, no. 5696, pp. 666–669, 2004.

[62] J. H. Warner, F. Schaffel, and M. Rummeli, *Graphene: Fundamentals and Emergent Applications*. Saint Louis, MO: Elsevier, 2012.

[63] V. Berry, "Impermeability of graphene and its applications," *Carbon*, vol. 62, pp. 1–10, 2013.

[64] J. Bai, X. Zhong, S. Jiang, Y. Huang, and X. Duan, "Graphene nanomesh," *Nature Nanotechnology*, vol. 5, pp. 190–194, March 2010.

[65] A. Sinitskii and J. M. Tour, "Patterning graphene through the self-assembled templates: Toward periodic two-dimensional graphene nanostructures with semiconductor properties," *Journal of the American Chemical Society*, vol. 132, no. 42, pp. 14730–14732, 2010. PMID: 20886879.

[66] Y. Lin, X. Han, C. J. Campbell, J.-W. Kim, B. Zhao, W. Luo, J. Dai, L. Hu, and J. W. Connell, "Holey graphene nanomanufacturing: Structure, composition, and electrochemical properties," *Advanced Functional Materials*, vol. 25, no. 19, pp. 2920–2927, 2015.

[67] Z. Xing, J. Tian, Q. Liu, A. M. Asiri, P. Jiang, and X. Sun, "Holey graphene nanosheets: Large-scale rapid preparation and their application toward highly-effective water cleaning," *Nanoscale*, vol. 6, pp. 11659–11663, 2014.

[68] X. Han, Z. Yang, B. Zhao, S. Zhu, L. Zhou, J. Dai, J.-W. Kim, B. Liu, J. W. Connell, T. Li, B. Yang, Y. Lin, and L. Hu, "Compressible, dense, three-dimensional holey graphene monolithic architecture," *ACS Nano*, vol. 11, no. 3, pp. 3189–3197, 2017. PMID: 28263560.

[69] S. D. Lacey, W. M. Van Cleave, X. Hua, D. Kirsch, V. Barone, Y. Lin, A. K. Gupta, and L. Hu, "Holey graphene gas separation membranes toward hydrogen-rich syngas." PowerPoint Presentation, May 2017.

[70] S. D. Lacey, "Re: Research publishing & holey graphene reduction question." Private Communication (Email), August 2017.

[71] S. D. Lacey, "Holey graphene SEM images." Unpublished Images, May 2017.

[72] J. Guan, S. Dorris, U. Balachandran, and M. Liu, "Transport properties of $BaCe_{0.95}Y_{0.05}O_{3-\alpha}$ mixed conductors for hydrogen separation," *Solid State Ionics*, vol. 100, no. 1, pp. 45–52, 1997.

[73] J. Mizusaki, K. Arai, and K. Fueki, "Ionic conduction of the perovskite-type halides," *Solid State Ionics*, vol. 11, no. 3, pp. 203–211, 1983.

[74] N. Bonanos, "Transport properties and conduction mechanism in high-temperature protonic conductors," *Solid State Ionics*, vol. 53, pp. 967–974, 1992.

[75] D. A. Stevenson, N. Jiang, R. M. Buchanan, and F. E. G. Henn, "Characterization of Gd, Yb and Nd doped barium cerates as proton conductors," *Solid State Ionics*, vol. 62, no. 3, pp. 279–285, 1993.

[76] N. Taniguchi, K. Hatoh, J. Niikura, T. Gamo, and H. Iwahara, "Proton conductive properties of gadolinium-doped barium cerates at high temperatures," *Solid State Ionics*, vol. 53, pp. 998–1003, 1992.

[77] J. Li, H. Yoon, T.-K. Oh, and E. D. Wachsman, "$SrCe_{0.7}Zr_{0.2}Eu_{0.1}O_3$-based hydrogen transport water gas shift reactor," *International Journal of Hydrogen Energy*, vol. 37, no. 21, pp. 16006–16012, 2012. Advances in Hydrogen Production (Selected papers from ICH2P-2011).

[78] R. H. Mitchell, *Perovskites: Modern and Ancient*. Thunder Bay, CAN: Almaz Press, 2002.

[79] F. S. Galasso, R. Smoluchowski, and N. Kurti, *Structure, Properties and Preparation of Perovskite-Type Compounds*. Oxford, UK: Pergamon Press-Elsevier, 1st ed., 2013.

[80] J. Zhu, H. Li, L. Zhong, P. Xiao, X. Xu, X. Yang, Z. Zhao, and J. Li, "Perovskite oxides: Preparation, characterizations, and applications in heterogeneous catalysis," *ACS Catalysis*, vol. 4, no. 9, pp. 2917–2940, 2014.

[81] G. C. Mather and M. S. Islam, "Defect and dopant properties of the $SrCeO_3$-based proton conductor," *Chemistry of Materials*, vol. 17, no. 7, pp. 1736–1744, 2005.

[82] T. Ishihara, *Structure and Properties of Perovskite Oxides*, ch. 1, pp. 1–16. Fuel Cells and Hydrogen Energy, Dordrecht, NED: Springer, 1st ed., 2009.

[83] A. Kruth, G. C. Mather, J. R. Jurado, and J. T. S. Irvine, "Anomalous variations of unit cell parameters with composition in proton conducting, $ACeO_3$-type perovskite solid solutions," *Solid State Ionics*, vol. 176, no. 7–8, pp. 703–712, 2005.

[84] J. Li, H. Yoon, T.-K. Oh, and E. D. Wachsman, "Stability of $SrCe_{1-x}Zr_xO_{3-\delta}$ under water gas shift reaction conditions," *Journal of The Electrochemical Society*, vol. 157, no. 3, pp. B383–B387, 2010.

[85] J. Li, H. Yoon, and E. D. Wachsman, "Carbon dioxide reforming of methane in a $SrCe_{0.7}Zr_{0.2}Eu_{0.1}O_{3-\delta}$ proton conducting membrane reactor," *International Journal of Hydrogen Energy*, vol. 37, no. 24, pp. 19125–19132, 2012. 2011 International Workshop on Molten Carbonates and Related Topics.

[86] A. Nowick and Y. Du, "High-temperature protonic conductors with perovskite-related structures," *Solid State Ionics*, vol. 77, pp. 137–146, 1995. Solid State Protonic Conductors VII.

[87] S.-J. Song, E. D. Wachsman, S. E. Dorris, and U. Balachandran, "Electrical properties of p-type electronic defects in the protonic conductor $SrCe_{0.95}Eu_{0.05}O_{3-\delta}$," *Journal of The Electrochemical Society*, vol. 150, no. 6, pp. A790–A795, 2003.

[88] K. D. Kreuer, "On the development of proton conducting materials for technological applications," *Solid State Ionics*, vol. 97, no. 1, pp. 1–15, 1997.

[89] E. Ostrovskiy, "Re: Membrane production." Private Communication (Email), April 2017.

[90] A. C. Makrides, M. A. Wright, and D. N. Jewett, "Separation of hydrogen by permeation." Patent, November 1967. US Patent 3,350,846.

[91] B. H. Howard, R. P. Killmeyer, K. S. Rothenberger, A. V. Cugini, B. D. Morreale, R. M. Enick, and F. Bustamante, "Hydrogen permeance of palladium-copper alloy membranes over a wide range of temperatures and pressures," *Journal of Membrane Science*, vol. 241, no. 2, pp. 207–218, 2004.

[92] K. S. Rothenberger, B. H. Howard, R. P. Killmeyer, A. V. Cugini, R. M. Enick, F. Bustamante, M. V. Ciocco, B. D. Morreale, and R. E. Buxbaum, "Evaluation of tantalum-based materials for hydrogen separation at elevated temperatures and pressures," *Journal of Membrane Science*, vol. 218, no. 1–2, pp. 19–37, 2003.

[93] U. Shigeyuki, K. Yukinori, S. Kohzoh, S. Noboru, M. Takeshi, and K. Eiichi, "A palladium/porous-glass composite membrane for hydrogen separation," *Chemistry Letters*, vol. 17, no. 10, pp. 1687–1690, 1988.

[94] S. Ilias, N. Su, U. I. Udo-Aka, and F. G. King, "Application of electroless deposited thin-film palladium composite membrane in hydrogen separation," *Separation Science and Technology*, vol. 32, no. 1–4, pp. 487–504, 1997.

[95] F. C. Gielens, R. J. J. Knibbeler, P. F. J. Duysinx, H. D. Tong, M. A. G. Vorstman, and J. T. F. Keurentjes, "Influence of steam and carbon dioxide on the hydrogen flux through thin Pd/Ag and Pd membranes," *Journal of Membrane Science*, vol. 279, no. 1–2, pp. 176–185, 2006.

[96] Aalborg, "GFC mass flow controller," 2017.

[97] Aalborg, *Operating Manual: GFC Mass Flow Controller*. Aalborg, December 2014.

[98] Omega Engineering, "Digital pressure gauges and models with alarm and analog outputs," 2017.

[99] Omega Engineering, *Revised Thermocouple Reference Tables*. Omega Engineering Inc., 2017.

[100] INFICON, *3000 Micro GC Gas Analyzer: Operating Manual*. INFICON, 2013.

[101] UL, "Polyethylene (PE) typical properties generic HDPE," 2017.

[102] T. D. Flaim, Y. Wang, and R. Mercado, "High-refractive-index polymer coatings for optoelectronics applications," in *SPIE Proceedings of Optical Systems Design* (C. Amra, N. Kaiser, and H. A. Macleod, eds.), vol. 5250 of *Advances in Optical Thin Films*, (St. Etienne, FRA), pp. 423–434, Society of Photo-Optical Instrumentation Engineers, September 2004.

[103] P. Arora and Z. J. Zhang, "Battery separators," *Chemical Reviews*, vol. 104, pp. 4419–4462, March 2004.

[104] L. Celgard, "Celgard 2325 product information," 2008.

[105] X. Zhang, K. K. Xiao, R. A. Nark, and R. E. Smith, "Microporous membrane separators for lithium ion rechargeable batteries and related methods." Patent Pending, November 2014. US Application US20160149181A1.

[106] C. van Rijn, M. van der Wekken, W. Nijdam, and M. Elwenspoek, "Deflection and maximum load of microfiltration membrane sieves made with silicon micromachining," *Journal of Microelectromechanical Systems*, vol. 6, pp. 48–54, March 1997.

[107] Engineering ToolBox, "Modulus of elasticity or young's modulus - and tensile modulus for common materials," 2017.

[108] Ineos, "Typical engineering properties of polypropylene," tech. rep., INEOS Olefins & Polymers USA, League City, Texas, US, April 2014.

[109] McMaster-Carr, "Product detail: Square-profile oil-resistant buna-n o-ring 1/8 fractional width, dash number 214," 2015.

[110] Swagelok, "PFA flexible tubing," 2017.

[111] Airgas, "Safety data sheet: Hydrogen," safety data sheet, Airgas, January 2017.

[112] Airgas, "Safety data sheet: Carbon dioxide," safety data sheet, Airgas, January 2017.

[113] Airgas, "Certificate of conformance: Argon, industrial grade," certificate of conformance, Airgas, September 2016.

[114] Working Group 1, *Guide to the Expression of Uncertainty in Measurement*. Joint Committee for Guides in Metrology, 1st ed., September 2008.

[115] H. Liu, Z. Chen, S. Dai, and D.-e. Jiang, "Selectivity trend of gas separation through nanoporous graphene," *Journal of Solid State Chemistry*, vol. 224, pp. 2–6, 2015.